Award Number: W81XWH-12-1-0251

TITLE: Therapeutic Role of Bmi-1 Inhibitors in Eliminating Prostate Tumor Stem Cells

PRINCIPAL INVESTIGATOR: Isaac Y. Kim, M.D., Ph.D.

CONTRACTING ORGANIZATION: New Jersey, University of Medicine and Dentistry of,
Robert Wood Johnson Medical School
Piscataway, NY 08854

REPORT DATE: October 2013

TYPE OF REPORT: Annual

PREPARED FOR: U.S. Army Medical Research and Materiel Command
Fort Detrick, Maryland 21702-5012

REPORT DOCUMENTATION PAGE

Form Approved
OMB No. 0704-0188

1. REPORT DATE	2. REPORT TYPE	3. DATES COVERED
October 2013	Annual	30 Sep 2012-29 Sept 2013

4. TITLE AND SUBTITLE

Therapeutic Role of Bmi-1 Inhibitors in Eliminating Prostate Tumor Stem Cells

5a. CONTRACT NUMBER

5b. GRANT NUMBER:
W81XWH-12-1-0251

5c. PROGRAM ELEMENT NUMBER

6. AUTHOR(S)
Isaac Kim, M.D., Ph.D.
Joseph Bertino, MD (Partnering PI),
Hatem E. Sabaawy, MD, PhD (Initiating PI).

E-Mail: kimiy@cinj.rutgers.edu

5d. PROJECT NUMBER

5e. TASK NUMBER

5f. WORK UNIT NUMBER

7. PERFORMING ORGANIZATION NAME(S) AND ADDRESS(ES)

New Jersey, University of Medicine and Dentistry of, Robert Wood Johnson Medical School
Piscataway, NJ 08854

8. PERFORMING ORGANIZATION REPORT NUMBER

9. SPONSORING / MONITORING AGENCY NAME(S) AND ADDRESS(ES)
U.S. Army Medical Research and Materiel Command
Fort Detrick, Maryland 21702-5012

10. SPONSOR/MONITOR'S ACRONYM(S)

11. SPONSOR/MONITOR'S REPORT NUMBER(S)

12. DISTRIBUTION / AVAILABILITY STATEMENT
Approved for Public Release; Distribution Unlimited

13. SUPPLEMENTARY NOTES

14. ABSTRACT

Prostate tumor-initiating cells (TICs) have intrinsic resistance to current therapies. BMI-1 (B-cell-specific MMLV insertion site-1) regulates stem cell self-renewal, and is over-expressed in TICs. We developed a combined immunophenotypic and time-of-adherence assay to identify human prostate TICs with increased BMI-1 expression. Tumor initiation and dissemination were consistently observed in the immune-permissive zebrafish microenvironment from collagen-adherent $\alpha2\beta1^{hi}/CD44^{hi}$ cells. Utilizing the zebrafish xenograft model, we identified the first known translational inhibitors of BMI-1 that target prostate TICs. BMI-1 inhibitors induced prostate cancer cell senescence, and G1 cell cycle arrest. Targeting of BMI-1 significantly reduced clonogenic, migration, and invasion abilities of TICs, and increased cellular senescence. Treatment of zebrafish and mouse xenografts with BMI-1 inhibitor reduced the metastatic potential of zebrafish TIC-derived xenografts, and inhibited tumor growth in mouse xenografts, respectively. Therefore, we have accomplished our first year's goal to demonstrate the beneficial effects of targeting prostate TICs with BMI-1 inhibitors. The next phase of studies will examine BMI-1 targeted therapy in combination with Taxotere and other recently approved therapies. These studies will allow us to accomplish the goals of this synergistic award between three laboratories (Sabaawy, Bertino, and Kim) to develop a therapeutic strategy for BMI-1 inhibitors in prostate cancer.

15. SUBJECT TERMS

16. SECURITY CLASSIFICATION OF:			17. LIMITATION OF ABSTRACT	18. NUMBER OF PAGES	19a. NAME OF RESPONSIBLE PERSON
a. REPORT	b. ABSTRACT	c. THIS PAGE			USAMRMC
U	U	U	UU	54	19b. TELEPHONE NUMBER *(include area code)*

CONTENTS

Preprint of Bansal et al., *Prostate*, in press. (manuscript and supplemental material).

A. INTRODUCTION

Prostate tumor-initiating cells (TICs) have intrinsic resistance to current therapies. BMI-1 (B-cell-specific MMLV insertion site-1) regulates stem cell self-renewal, and is over-expressed in TICs. We developed a combined immunophenotypic and time-of-adherence assay to identify human prostate TICs with increased BMI-1 expression. Our goal is to identify and subsequently develop a new class of bioavailable small molecules that inhibit tumor growth by selectively reducing BMI-1 production. The approved statement of work (SOW) described synergistic efforts of three laboratories; that of the initiating PI (Hatem Sabaawy, MD, PhD; contract #W81XWH-12-1-0249); partnering-PI (Joseph Bertibo, MD; contract #W81XWH-12-1-0250); and partnering-PI (Isaac Kim, MD, PhD; contract #W81XWH-12-1-0251) to ensure the achievement of this goal.

Tow central elements are investigated in parallel in the three laboratories for this project; 1) Drug screening for BMI-1 inhibitors utilizing zebrafish (Sabaawy Lab), prostate cancer cell lines (Bertino Lab), and primary prostate tissue xenografts (Kim Lab). 2) Once compounds are identified as candidate BMI-1 inhibitors, these compounds will be further assessed for their effects on primary prostate tumor initiation and maintenance. Candidate compound antitumor activity will be investigated in zebrafish (Sabaawy Lab) and mice xenografts (Bertino Lab) of primary prostate cancer tissue (Kim Lab). The following tasks from **the approved SOW** were performed to achieve the goal of defining the strategy for use of effective BMI-1 inhibitors in future trials:

Task #1. Evaluate the expression of markers of TICs such as BMI-1 and CD44 and correlation with prostate cancer markers in prostate cancer patients using IHC. We demonstrated the correlation of BMI-1 and CD44 expression in TICs in the accomplished tasks section below (Fig. 1), and correlation of TICs expression to PCa markers AMACR[1] and Erg in the published manuscript[2] (see appendix).

Task #2. Isolate and characterize TICs from prostate cell lines and primary prostate tumor tissues. TICs were isolated at the partnering PI (Bertino Lab and Kim Lab) in coordination with our medical oncology collaborators. We isolated TICs from the primary prostate tumor tissue and confirmed the tumor initiation ability of collagen attached TICs in nude mice (Bertino lab) and zebrafish (Sabaawy lab)[2] (see appendix).

Task #3. Evaluate BMI-1 compounds as inhibitors of TICs from fresh human prostate tumors using *in vitro* functional assays. We performed collagen adherence assays (Bertino Lab); drug combination assays (Bertino Lab and Sabaawy lab); inhibition of growth of prostaspheres (Bertino Lab); and tested growth of collagen adherent TICs. The results are displayed in the accomplished tasks section below (Fig. 2-3 for testing TICs), (Fig. 4 for a novel finding of the role of BMI-1 in metastasis), (Fig. 5 for combination and chemotherapy effects on TICs), (Fig. 6-9 for effects of BMI-1 inhibitor C-209 on collagen adherence, prostaspheres, and tumor growth).

The following three additional tasks were listed under year 2, but continue during the first 2 years.

Task #4. This task was listed in approved SOW to continue from year 1 through year 2 (months 4-24). We have established models of primary prostate xenografts from TICs in zebrafish (Sabaawy Lab) and mice (Bertino Lab)[2] (see appendix). This task will continue in year 2 using additional primary samples.

Task #5. This task was listed in approved SOW to continue from year 1 through year 2 (months 4-24). We have evaluated the toxicological profile of selected BMI-1 inhibitors (C-209, C-210, and C-211) in zebrafish embryos and their antitumor effects in xenografts (see Fig. 6-9 for effects of BMI-1 inhibitor C-209). We will continue to perform toxicological assays for BMI-1 inhibitors in the second year of the project.

Task #6. This task was listed in SOW to continue from year 1 through year 2 (months 4-24). We performed toxicity and antitumor effects of BMI-1 inhibitors in zebrafish (Sabaawy Lab) (Fig. 6-9 for effects of C-209).

From the above experiments performed in the first year of the project, we are on track for determining which BMI-1 inhibitor(s) to be used for *in vivo* studies in NOD-SCID mice and fish during the second and third years of the project to determine the most effective combination therapy for use of BMI-1 inhibitors for PCa therapy. We have published one manuscript[2] (see appendix) from the studies of the first year and generated more data for additional manuscripts on the development and characterization of BMI-1 inhibitors that will be completed during the next two years of the project.

B. BODY

Treatment of advanced prostate cancer (PCa) has been challenging with limited success[3]. Although several agents such as abiraterone, cabazitaxel, denosumab, sipuleucel-T became available during the last few years for managing castration resistant PCa (CRPC), these therapies only marginally extend median survival by ~3 months[4,5], and resistance to these treatments are emerging. There is a dire need for therapies that are safe, efficacious, and cost-effective for treating CRPC, and can be used in early disease to prevent metastasis.

It is ever more accepted that fractions of PCa cells acquire and/or retain tumor initiation and self-renewal potentials, therefore are termed TICs[6,7]. We have identified prostate TICs from primary tissues that are collagen-adherent $\alpha2\beta1^{hi}$/$CD44^{hi}$ cells[2] (see appendix). Recent experimental and clinical studies have identified BMI-1 as a member of the polycomb family of chromatin remodeling complexes that act as transcriptional repressors for epigenetic chromatin modification. BMI-1 encodes a zinc finger protein that forms a key rate-limiting regulatory component of the polycomb repressor complex (PRC1) regulating cellular transcription. PRC1 enzymatic activities include DNA methylation of CpG islands and global mono-ubiquitination of histone 2A. Our data demonstrate that upregulated BMI-1 levels correlate with advanced PCa. PCa TICs can self-renew and also generate non-TIC progeny[6]. Prostate TICs survive treatment due to their intrinsic resistance to current therapies[8,9]. BMI-1 is a central player in PCa progression as it controls growth signals[10-15], regulates oncogenic microRNAs[16], and induces metastasis markers [17]. BMI-1 is overexpressed at levels much higher in cancer cells vs. normal cells[18] (Preliminary data) (Fig. 1)**,** and contributes to therapy resistance, in particular in advanced and/or metastatic PCa[10,18,19]. Importantly, the strongest BMI-1 expression is observed in tissues[20,21], and plasma[22-25] of highly aggressive tumors undergoing metastasis. Notably, BMI-1 protein levels in serum of PCa patients correlate with increased serum PSA[26]. Therefore, BMI-1 is an excellent biomarker for advanced PCa, and targeting BMI-1 is a compelling therapeutic approach.

Knockdown of BMI-1 inhibits cell proliferation and results in growth arrest[11]; whereas its overexpression promotes anchorage independent growth and cell invasion[12]. With recent sequencing of pancreatic and kidney cancers[27,28] and determination of mutational landscape of PCa[29], an unexpected intratumor heterogeneity was revealed. A common feature of these heterogeneous clones is self-renewal, a feature that can be effectively targeted by inhibiting BMI-1.

We identified primary PCa adherent $\alpha2\beta1^{hi}$/$CD44^{hi}$ TICs in mouse and zebrafish xenografts[2] (see manuscript in appendix) that overexpress BMI-1 (see accomplished tasks below; Fig. 1). TICs are comprised of heterogeneous subpopulations with multiple phenotypes[30]. Prostate TICs and invasive cells are enriched for CD44[31] (accomplished tasks; Fig. 1), suggesting an intriguing mechanism of initiating PCa invasion though basement membrane degrading activity of $CD44^{hi}$ TICs. BMI-1 promotes prostate tumorigenesis by several mechanisms, including repressing $p16^{Ink4a}$ and ARF genes regulating senescence. We demonstrate that BMI-1 inhibitors target these senescence targets (accomplished tasks; Fig. 8). In summary, BMI-1 is a critical target in PCa and developing BMI-1 inhibitors will provide novel and effective therapy for PCa treatment.

C. ACCOMPLISHED TASKS

Task1. Evaluation of BMI-1 expression in PCa. BMI-1 is a potential target for human prostate TICs. We examined whether BMI-1 is upregulated in prostate cancer cells, and whether it is coexpressed with the putative prostate TIC marker CD44 in primary prostate cancer tissues. To evaluate the clinical relevance of BMI-1 activation, we conducted *BMI-1* and *CD44* expression analyses on FFPE human PCa by IHC (Fig. 1). Clinical tissues were classified according to postoperative Gleason score or clinical stage (TNM system). Histological categories divided tumors with Gleason scores, whereas clinical stage groups were defined as prostate-confined disease (pT2) and disease with extraprostatic extension (pT3). First, PCa regions were identified with the granular cytoplasmic staining of AMACR[1] and ERG overexpression when TEMPRSS-ERG fusion was detected [2] (please see supplemental figures in the appendix). Sequential sections were then examined for expression of CD44 (progenitor isoform) and BMI-1. Early-stage adenocarcinomas showed upregulated BMI-1 and CD44 coexpression, as compared to normal margins (Fig. 1, top representative sections, n=17, 12/17 **(70%)** demonstrated the same pattern) (Fig. 1). These data from TMA were also seen in tissues from eight patients who were recruited to this study (Table 1), are consistent with previous reports[10,18,19,26], and suggest that PCa patients would benefit from BMI-1-targeted therapies.

1ry prostate	Age	Type	Grade	pTNM	Gleason	R2	99% confidence	TIC frequency
15728	62	Adc	3	pT2c	3 + 3	0.999	1/7 to 1/37	1/16
17148	52	Adc	3	pT2c	3 + 3	0.995	1/29 to 1/153	1/71
17761	57	Adc	3	pT2c	3 + 3	0.995	1/64 to 1/228	1/120
19803	55	Adc	3	pT2c	3 + 3	0.999	1/59 to 1/456	1/185
24126	53	Adc	4	pT3a	3 + 3	0.995	1/32 to 1/114	1/36
40181	60	Adc	4	pT3a	3 + 4	0.998	1/29 to 1/153	1/71
25185	67	Adc	3	pT2c	3 + 3	ND	ND	ND
25315	66	Adc	4	pT3a	3 + 4	ND	ND	ND
26136	67	Adc	3	pT3b	4 + 5	0.995	1/4 to 1/47	1/8
25854	55	Adc	4	pT3b	4 + 5	0.998	1/7 to 1/37	1/16
28838	65	Adc	P	P	P	P	P	P
28864	66	Adc	P	P	P	P	P	P
28869	67	Adc	P	P	P	P	P	P
29032	68	Adc	P	P	P	P	P	P
29084	67	Adc	P	P	P	P	P	P
29092	66	Adc	P	P	P	P	P	P
29110	69	Adc	P	P	P	P	P	P

Table 1. Primary prostate cancer patient characteristics and TIC frequency. Table shows data from seventeen patients recruited with number of each case, age, prostate cancer type (adc, adenocarcinoma), histological grade, pathological staging based on the pTNM classification, where pT2c indicates bilateral prostate disease, and total Gleason scores. TIC frequencies of 1/16 (6.25%), 1/71 (1.4%), 1/120 (0.83%), 1/185 (0.54%), 1/36 (2.7%), 1/71 (1.4%), 1/8 (12.5%), 1/16 (6.25%), and a frequency range of 0.22% to 25.0% were calculated in the eight patient samples using ELDA with 99% confidence interval, and with the displayed correlation coefficient (R2) values. ND, not done due to limited tissues. P, pending.

Task2. Isolation of prostate TICs using phenotypic and time-of-adherence assay. As compared to CSCs or TICs from other solid tumors, few studies have reported on the isolation of primary human prostate TICs, likely due to the limited availability of sizable primary tumor tissues. Our experimental approach allowed us to identify prostate TICs using a combination of time-of-adherence and phenotypic assays (Fig. 2A). We isolated $CD44^{hi}$ and α2β1-$integrin^{hi}$ prostate TICs from prostatectomy tissues and PCa cell lines upon enrichment with collagen adherence [2] (see appendix).

On the basis of rapid adhesion on collagen, PCa cells were plated on a collagen-I dish for 5 min (5'=rapidly adherent) (3-5% of cells) were enriched for TICs by sorting the $\alpha_2\beta_1^{hi}/CD44^{hi}$ cells. The sorted adherent cells upregulated CD133 (From 0.01% to ~3%), and this fraction showed superior ability to form tumors in mice[2] (see appendix). The $\alpha2\beta1^{hi}/CD44^{hi}$ cells have significantly higher colony forming efficiency, increased migration, and increased invasion abilities vs. $\alpha2\beta1^{low}/CD44^{low}$ cells[2]. The ability of the $\alpha2\beta1^{hi}/CD44^{hi}$ TICs to self-renew was tested in serial spheroid assays. Disaggregated primary spheroids from $\alpha2\beta1^{hi}/CD44^{hi}$ cells reformed spheroids in 2^{ry} and 3^{ry} assays, whereas those from $\alpha2\beta1^{low}/CD44^{low}$ cells formed only cell clusters in 2^{ry} assays, reflecting their limited stemness[2]. Thus, adherent $\alpha2\beta1^{hi}/CD44^{hi}$ cells are more tumorigenic *in vitro*, and in mice, therefore fulfilled the criteria of TICs.

Expression of CD44, α2β1-integrin, and CD133 in each fraction was analyzed. The 5 min-adherent cell fraction had an average of several fold higher number of cells highly coexpressing α2β1 and CD44 as compared to the 20 min-non-adherent in PC3 and CWR22 cells examined (Fig. 3A). Thus phenotypically, the 5 min-adherent fraction is enriched in $\alpha2\beta1^{hi}/CD44^{hi}$ cells, while the 20 min-non-adherent fraction comprise $\alpha2\beta1^{low}/CD44^{low}$ cells (Fig. 3B). When cells from the 5 min-adherent fraction of PC3 and CWR22 cells that are α2β1hi/CD44hi cells were grown as prostate spheres, known to contain putative TICs that can initiate serially passageable spheres, the consistently low CD133 expression increased, and up to 5% of the cells were CD133 (Fig. 3C), while CD133 was still undetectable in LNCap cells when grown as prostate spheres. Thus, we conclude that in primary prostate cancer cases (n=6), the 5 min-adherent fraction was enriched in $\alpha2\beta1^{hi}/CD44^{hi}$ cells, and in CD133+ cells when grown as prostate spheres, compared to the non-adherent fraction.

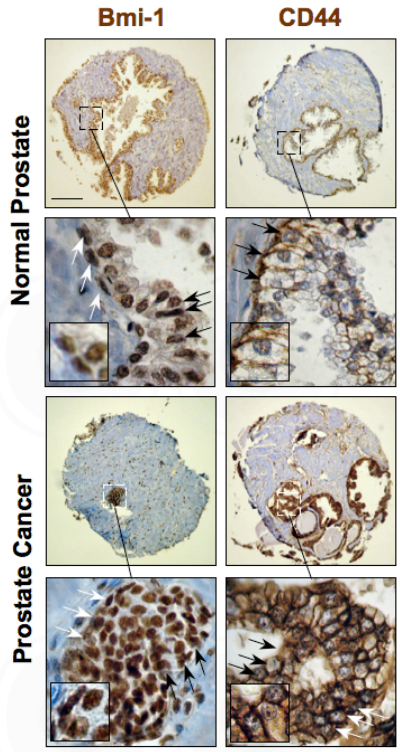

Figure 1. Expression of Bmi-1 and CD44 in diagnostic sections from prostate cancer patient. IHC staining of sections from primary human prostate cancer patients undergoing prostatectomy showing upregulation of both Bmi-1 (insert with nuclear staining in brown on the left), and CD44 (insert with membrane staining in brown on the right) in tumor tissue (lower panels) vs. normal prostate margin (upper panels). Arrows indicate expression of Bmi-1 and CD44 in both basal (white arrows) and luminal layers (black arrows). Scale bars are 200 μm, and 20 μm in magnified panels.

To generate a xenograft model for studying primary prostate TICs' response to therapy, we developed methods to track primary human cells in the translucent zebrafish using Quantum Dots (QDs). We labeled TICs from six primary prostatectomy tissues, and multiple PCa cell lines with QDs at the narrow 605 red emission with near 100% efficiency. To show proof-in-principle that TICs initiate tumors *in vivo* in zebrafish, we injected them with QD-labeled TICs[2]. Embryonic grafts were performed at pre-immune stages before development of fish cell-mediated immunity in a more immune-permissive environment to allow for testing of full tumor initiation potential**.** This was critical as recent reports suggested that tumor cells initiate more tumors in more immune-permissive NOD-SCID-IL2-γ (NSG) than NOD-SCID mice. We isolated TICs by adherence to collagen strategy (Fig. 2A), labeled them with QDs, and injected them into 48-hour post fertilization (hpf) embryonic zebrafish, or in conditioned juvenile fish. Human primary PCa cells and cell lines labeled with QDs formed

localized tumor graft in 4-day embryos (Fig. 2B) that often disseminated to metastatic sites[2]. Importantly, normal CD44$^{-/low}$ non-adherent stem cells from same patient survived, but failed to initiate tumors. Transplanted cells were traceable *in vivo* in living fish[2]. Prostate TICs proliferated, and initiated visible tumors on average after 13 days, and then invaded tissues, and formed distal metastasis by day 28[2]. Cells from patients with CRPC were monitored and seen to more frequently metastasize to distal sites[2] similar to human PCa.

We previously demonstrated in the preliminary data of the application that sections of xenografts demonstrate metastatic colonies detected at the kidney marrow of zebrafish (Fig. 4A), the site analogous to human bone marrow. We have now determined that BMI-1 is directly involved in the metastatic process *in vivo* by performing IHC analysis of localized vs. metastatic colonies in sections from six different PCa xenografts. Fish with metastatic grafts determined by disseminated QD IF appearance were fixed, and sections were examined. In primary PCa graft masses, 50±8% of cells express BMI-1 (Fig. 4B), in contrast to 89±4**%** of tumor cells expressing BMI-1 in metastatic colonies (Fig. 4B, $p<0.01$). These data support a novel role for BMI-1 in driving PCa metastasis.

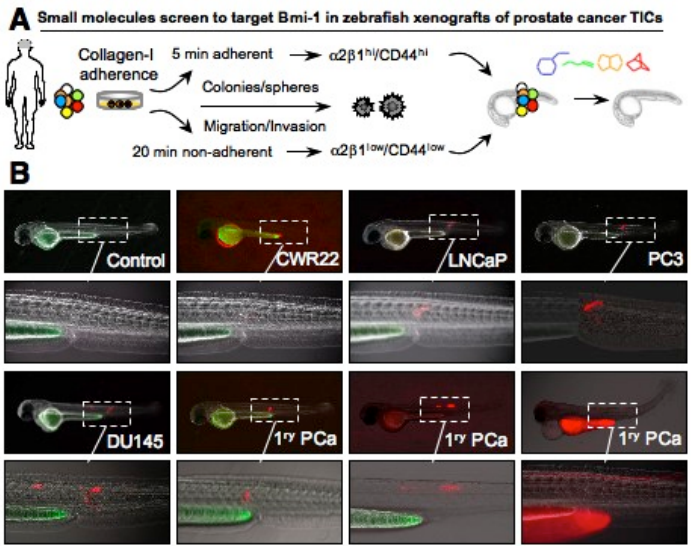

Figure 2. Prostate TICs xenotransplants in embryonic zebrafish. *(A) Schematic illustration of experimental procedure allowing for the testing of combination therapy in zebrafish xenografts of primary PCa. TICs were separated by collagen adherence, sorted for integrin/CD44, and then subjected to in vitro clonogenic, migration, and invasion assays, or injected in zebrafish embryos. (B-E) Bright field (B, D) and red 605 fluorescent (C, E) images from embryos transplanted with TICs with brain metastasis (arrows in D-E). Images were taken 9 days post-transplantation. (F-H) H&E (F, I), and anti-human CD44 IHC (G-H) in control (F-H), and xenotransplant embryo with brain metastasis (I-K).*

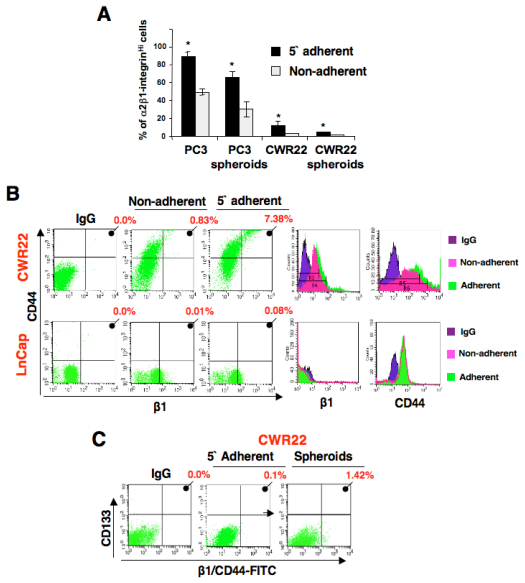

Figure 3. Collagen-adherent cells are enriched in putative TICs. A, Mean percentage of 5` adherent and 20` non-adherent cells in PC3, PC3 spheroids, CWR22, and CWR22 spheroids. Data represent three independent experiments. **B,** Flow cytometric analyses of CWR22 and LnCap cells after collagen adherence showing higher mean fluorescence intensity (MFI) of 5 minutes collagen-I-adherent (α2β1^{hi}/CD44^{hi}) cells (Adherent) compared to 20 min-non-adherent (α2β1^{low}/CD44^{low}) cells (Non-adherent), and IgG control (IgG). **C,** CD133 expression in various subsets of CWR22 cells. In a representative experiment, 0.1% of the cells were CD133 positive, and spheroids from upregulated CD133 to 1.42% (*$p<0.001$).

Task3. Evaluate BMI-1 inhibitors in targeting prosate TICs.

To determine if the 5 min-adherent cell fraction contains TICs, α2β1hi/CD44hi DU145 cells within this fraction were examined by colony formation, and migration and invasion assays. Cells within the 5 min-adherent cell fraction with an α2β1^{hi}/CD44^{hi} phenotype showed a nearly 2-fold higher colony formation, and increased migration and invasion abilities as compared to α2β1^{low}/CD44^{low} cells[2] (see appendix).

An essential characteristic of TICs is their ability to self-renew in serial plating assays. The α2β1^{hi}/CD44^{hi} DU145 cells formed significantly more single cell-derived spheroids as compared to α2β1^{low}/CD44^{low} cells. Moreover, spheroids formed from α2β1^{low}/CD44^{low} DU145 cells were fewer after day-5, and stopped growing after day-9 (Fig. 5A-B) suggesting that these cells lack self-renewal abilities. To assess self-renewal at an earlier time point of sphere formation, single cells derived from day 7-primary spheroids were replated for secondary spheroid formation assays. Once again, α2β1^{hi}/CD44^{hi} DU145 cells generated significantly more spheroids than α2β1^{low}/CD44^{low} cells (Fig. 5C). Collectively, the α2β1^{hi}/CD44^{hi} prostate cancer

cells exhibit enhanced tumorigenic, invasive, and self-renewal abilities.

TICs were shown to be resistant to chemotherapies. Since we isolated putative TICs by collagen adherence, we hypothesized that treatment with drugs that target TICs would reduce the number of cells adhering to collagen-I. Hence, we performed the collagen adherence assay upon treatment with chemotherapies commonly used for prostate cancer at IC_{50s} established by MTS assays (Fig. 5D). Indeed, the number of PCa collagen-adherent cells was not affected by chemotherapy treatments (Fig. 5E), and on the contrary increased with methotrexate and carboplatin (Fig. 5E) suggesting that these agents that are frequently used in the clinic for cancer treatment might increase the percentage of putative TICs.

An essential property of TICs is their ability to initiate tumor growth in immune-compromised mice with limited cell numbers. We tested whether the 5 min-adherent DU145 cells are more tumorigenic. Cells were injected SC in the abdominal flanks of nude mice. Tumors were analyzed by three variables: tumor incidence, tumor growth rate (mm^3/day), and final tumor volume (mm^3; Fig. 2B in [2] (see appendix)). Only 17% of mice (n=3/20) injected with non-adherent cells developed tumors, while nearly all mice injected with either adherent (n=18/20) (90%) or total DU145 cells (n=17/20) (85%) developed tumors. Mice injected with adherent cells developed tumors as early as 15 days post-transplantation, compared to day 35 for mice injected with the same cell dose of one million total DU145 cells. In an additional experiment, injection of only 1,000 adherent cells resulted in tumor formation and tumor volumes that were significantly larger than those generated by injections of one million total DU145 cells. After 50 days of growth, adherent DU145 tumors reached an average final volume of 867 mm^3. This was significantly larger than non-adherent and total DU145 tumors, which reached final volumes of 126 and 338 mm^3, respectively (P values are 0.0006 and 0.0001, respectively, when compared with adherent cell tumors). Thus, the $\alpha2\beta1^{hi}/CD44^{hi}$ DU145 cells are more tumorigenic in mice.

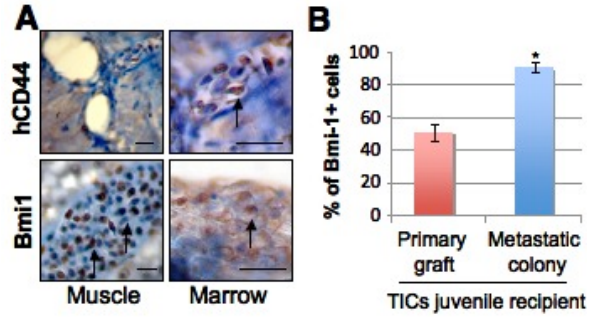

Figure 4. IHC of PCa xenografts in zebrafish. *A. TICs expressing BMI-1 (arrows). B. Marrow metastasis with many BMI-1-positive metastatic human cells.*

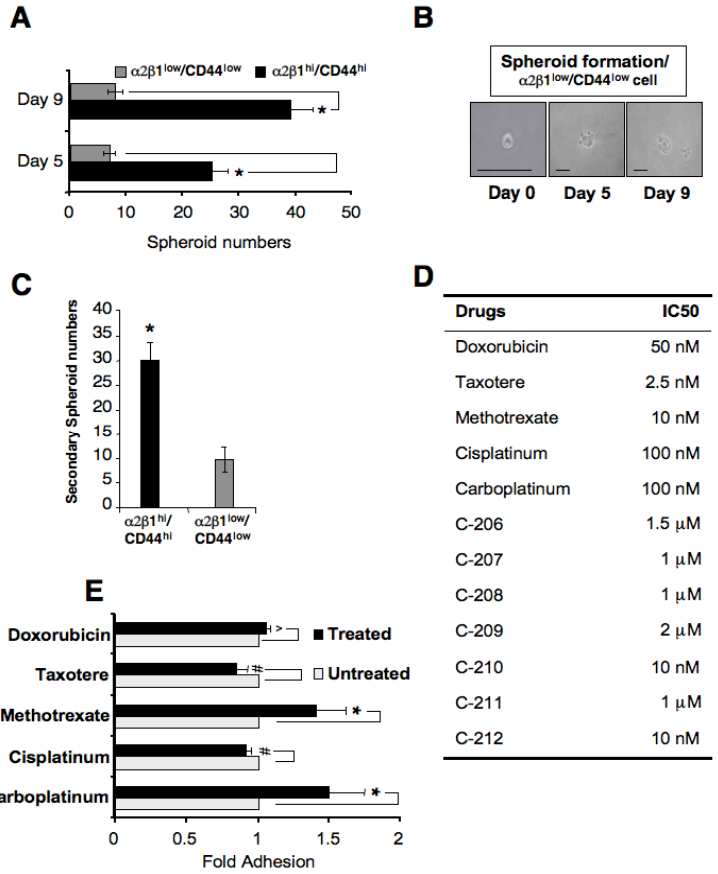

Drugs	IC50
Doxorubicin	50 nM
Taxotere	2.5 nM
Methotrexate	10 nM
Cisplatinum	100 nM
Carboplatinum	100 nM
C-206	1.5 μM
C-207	1 μM
C-208	1 μM
C-209	2 μM
C-210	10 nM
C-211	1 μM
C-212	10 nM

Figure 5. Self-renewal and *in vitro* tumorigenic potential of collagen-adherent $\alpha2\beta1^{hi}/CD44^{hi}$ cells. A, Bars demonstrate the enhanced ability of single $\alpha2\beta1^{hi}/CD44^{hi}$ cells to form spheroids, compared to the limited ability of single $\alpha2\beta1^{low}/CD44^{low}$ cells. **B,** Images from $\alpha2\beta1^{low}/CD44^{low}$-derived spheroids that stopped growing at day 9. Scale bars are 50 μm. **C,** Quantitation of secondary spheroids from $\alpha2\beta1^{hi}/CD44^{hi}$ and $\alpha2\beta1^{low}/CD44^{low}$ single cells derived from primary spheroids at day-7. Numbers of spheroids are displayed as mean ± s.e.m, and were done in triplicate. **D,** IC_{50} concentrations of various drugs and Bmi-1 inhibitors used. IC_{50}s were determined using MTS assays in DU145 cells. **E,** DU145 cells were treated with clinically used chemotherapy drugs at IC_{50} concentrations. Collagen-adherent cells at 5-minutes were measured using MTS assays. Values denote mean fold of 5 minute-adhesion ± s.d from three independent experiments. There was a lack of significant inhibition of 5 min-adhesion with taxotere and cisplatinum (#$p>0.05$), non-significant increase in adhesion with doxorubicin (^$p>0.05$), and statistically significant increase in adhesion with methotrexate and carboplatinum (* $p<0.05$) suggesting resistance.

Task4. Drug discovery of BMI-1 inhibitors. To investigate if pharmacological targeting of BMI-1 would provide a potential therapy to target prostate TICs, we screened a small molecule library (from PTC Therapeutics) for inhibitors of BMI-1 utilizing both luciferase- and GFP-reporters encompassing the 5`UTR and 3`UTR of BMI-1[32]. These small molecules selectively bind to BMI-1 mRNA, and modulate post-transcriptional expression of BMI-1 protein [32]. They were selected based on their 3-D chemical structure[32], and were synthesized by Rutgers chemistry group for clinical applications. After screening hundreds in fish and cell reporter assays, compounds with superior kinetics, toxicity, and efficacy in BMI-1 knockdown were identified. The IC_{50} values were determined using MTT assays. We used fish embryonic toxicology assays to show that selected compounds have no toxicity *in vivo*, and do not affect embryonic ESCs (not shown). Toxicology assays allowed us to select a number of small molecules for further testing (C-209 and ten derived molecules). These small molecules inhibited the expression of BMI-1 in DU145 cells and primary cells (Fig. 6), with the expected reduction in downstream ubiquitinated γ-H2A levels. Other growth related proteins assessed were unaffected (e.g. p27, H2A, Fig 7B). To study the mechanisms by which BMI-1 inhibitors induce tumor cell killing, cell cycle analyses were examined and demonstrated that BMI-1 inhibitors induced a dose-dependent G1 arrest in DU145 cells. Previous RNAi studies suggested that normal stem cells are more tolerant to reduced BMI-1 levels than tumor cells.

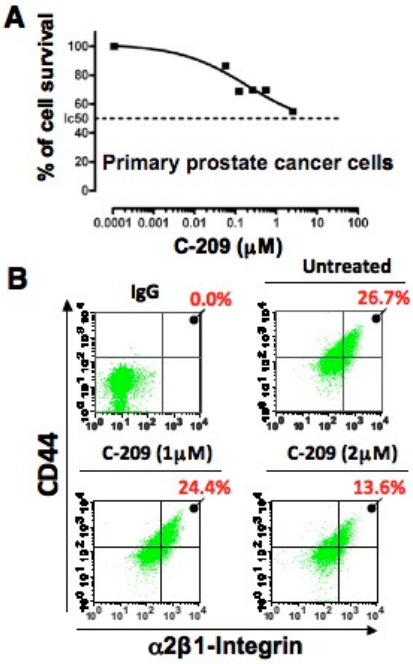

Figure 6. Activity of BMI-1 inhibitor in 1^{ry} PCa cells. A, IC_{50} for C-209 averaged 1-3 micromole in 1^{ry} PCa cells. **B,** Flow cytometry panels showing that treatment with C-209 targets $\alpha2\beta1^{hi}/CD44^{hi}$ TICs in a dose-dependent manner.

Indeed, we found tumor cell proliferation is more sensitive to BMI-1 reduction than that of normal progenitor cells ($CD34^{+}$ HSCs), in colony assays, providing a favorable safety margin for C-209. The selectivity of C-209 was investigated by profiling it against both a library of purified kinase targets using Z'-LYTE SelectScreen profiling assay (Invitrogen) against 245 kinases, and phosphatase profiler with an IC_{50} profiler (Millipore). Both assays yielded <10% activity for C-209.

BMI-1 suppression in primary collagen-adherent cells (putative TICs) at low concentrations resulted in a significant PCa killing (Fig. 6A), and significantly reduced the percentages of $\alpha2\beta1^{hi}/CD44^{hi}$ prostate TICs in a dose-dependent fashion (Fig. 6B). We also performed high-throughput toxicology assays in zebrafish embryos to determine a safe IC_{50}. Two compounds C-209, and C-210 had no toxic effects on zebrafish embryonic stem cells when used at IC_{50} established in human PCa cells, and C-209 is effective in targeting self-renewal in PCa xenografts.

Treatment with C-209 significantly reduced the number of single cell-derived colonies in secondary spheroid assays (Fig. 7A), in contrast to slight inhibitory effects of

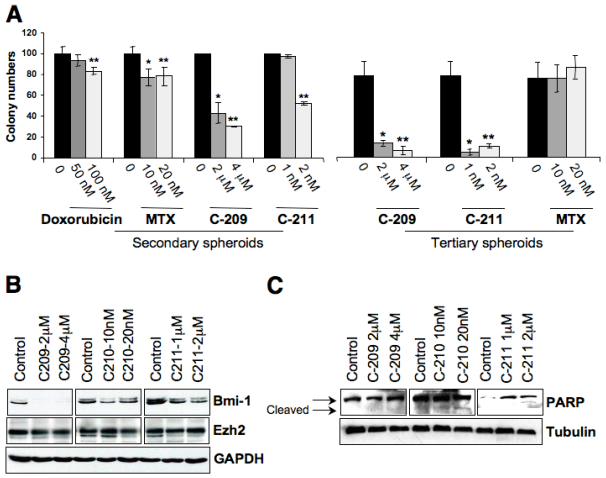

Figure 7. Characterization of BMI-1 inhibitors. A, The effects of Bmi-1 inhibitors vs. methotrexate (MTX) and doxorubicin on the formation of secondary and tertiary spheroids from single cells. Data represent three independent experiments using IC_{50} concentrations (*), and 2x IC_{50} concentrations (**), and treatments were found to be statistically significant where indicated (*, **P<0.005 compared to untreated). **B,** Western blot analysis of BMI-1 and Ezh2 levels in DU145 cells treated with C-209-211 at 1x and 2x of the IC_{50} concentrations. GAPDH levels were used as controls. **C,** Western blot analysis of total and cleaved (lower arrow) PARP levels in DU145 cells treated with C-209-211 at indicated concentrations. Tubulin levels were used as controls.

methotrexate and doxorubicin. Importantly, the effects of C-209 and C-211 treatment on tertiary colony formation from spheroids at day 7 were remarkable in reducing colony formation by nearly 10-fold, while methotrexate had no effect (Fig. 7A) suggesting that inhibiting BMI-1 might eliminate self-renewal of prostate TICs.

These three compounds were further pursued, and they effectively targeted BMI-1 (Fig. 7B). The effects were specific to BMI-1, but not to other PRC1 complex proteins such as Ezh2 (Fig. 7B). To validate that C-209 has activity against the putative TIC fraction in other prostate cancer cells, we treated PC3, CWR22 and LNCap cells with C-209. This treatment resulted in a significant reduction in the 5-min adherent $\alpha2\beta1^{hi}/CD44^{hi}$ cells suggesting that C-209 might be targeting this TIC fraction. To further validate the specificity of these compounds, we treated mouse embryonic fibroblasts (MEFs) that are either Bmi-$1^{+/+}$ or Bmi-$1^{-/-}$ with the three compounds. Since Bmi-1 knockdown was shown to induce senescence, we measured senescence in MEFs by staining with β-gal. C-209, C-210, and C-211 treatment elicited a significant increase in senescence of the Bmi-$1^{+/+}$ MEFs compared to untreated cells, and these effects were not significant in the highly senescent Bmi-$1^{-/-}$ MEFs (Fig. 8D-E). Moreover, knockdown of BMI-1 using shRNA resulted in a significant increase in senescence of DU145 cells (Fig. 8D-E) further validating BMI-1 as a target for pharmacological inhibition in prostate cancer cells.

C-209 is a translational inhibitor of BMI-1 expression that was chemically derived by substituting the aminothiazole derivative at position 4 with an imidazolopyrymidine. C-209 was most effective in inhibiting cell proliferation by selectively targeting BMI-1 in DU145, PC3 and CWR22 cells, and reducing the ubiquitinated form of H2A, a product of the BMI-1 PRC1 complex (Fig. 7), and by increasing senescence (Fig. 8D-E).

We further investigated other potential mechanisms by which C-209 increased senescence and induced killing of prostate cancer cells. Cleavage of PARP indicates activation of the apoptotic pathway. Similar levels of PARP cleavage were detected in treated and control cells (Fig. 7C). Since Bmi-$1^{-/-}$ MEFs display high levels of senescence, we examined the senescence levels in other prostate cancer cell lines after treatment with C-209 (Fig. 8A-B). Treatment with C-209 elicited a significant dose-dependent increase in senescence of DU145 cells (cells with the highest BMI-1 expression levels among prostate cancer cell lines examined) compared to PC3, LNCap, and CWR22 cells (Fig. 8B). In contrast, treatment of LNCap cells with C-209 resulted in a significant decrease in senescence. While the mechanisms by which C-209 effects on senescence in LNCap cells requires further investigations, differences in BMI-1 levels, androgen receptor status, and RB status might contribute to the difference in senescence

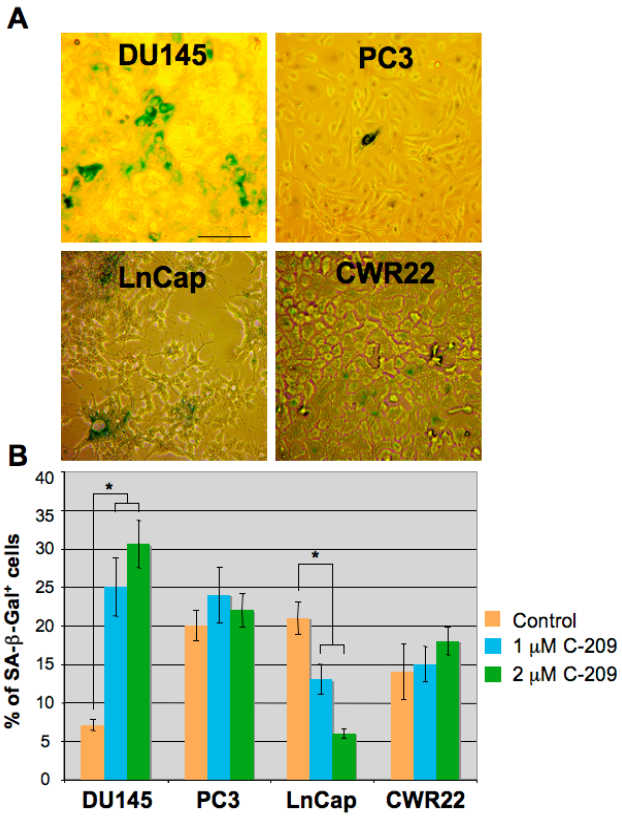

Figure 8. BMI-1 inhibitor increases senescence. SA-β-gal staining of cells from multiple prostate cancer cell lines treated with C-209. **A,** representative images of SA-β-gal staining of the indicated prostate cancer cell lines after treatment with C-209. Scale bar is 50 μm. **B,** Quantitation of SA-β-gal staining in control and C-209-treated cells. (*$p<0.05$ compared to untreated cells). Treatment resulted in significant increase in senescence of DU145 cells. In contrast, LnCap cells showed a significant decrease in senescence. Data are from two experiments performed in two 6-well plates for each treatment. Percentage of senescent cells was determined based on counts of 1,000 cells per treatment.

responses. We will further investigate these differences in primary prostate cancer tissues to determine if the same variability in senescence occurs in patients' samples.

Since we determined the IC_{50} of C-209 in DU145 cells to be 2 μM, we examined the IC_{50} of C209 in LNCap cells, and found it to be 1 μM (Fig. 9A-B). We next examined the effects of treatment with C-209 on cell invasion. C-209 treatment resulted in a significant decrease in cell invasion in both DU145 and LNCap cells at higher concentrations (Fig. 9C). Furthermore, C-209 displayed potent antitumor activity against the 5-min adherent $\alpha2\beta1^{hi}/CD44^{hi}$ DU145 sphere-forming cells (TICs) that we have shown to have higher BMI-1 expression, when used in spheroid assays (Fig. 9D). These studies demonstrate that the antitumor activity of C-209 correlates with the levels of expression of BMI-1. The selectivity of C-209 was further validated by lack of significant inhibition of a panel of 160 kinase and 21 phosphatase.

To address any concern that BMI-1 inhibitors might act differently in mammalian systems and mouse models of PCa, we used PCa mouse xenografts to examine the antitumor activity of C-209. The initial experiment was performed using mice bearing well-established DU145 tumors and treated with C-209 for 10 days. This treatment resulted in a 65% reduction of tumor growth. To show selectivity of C-209 against BMI-1, we measured intratumor levels of BMI-1 and non-specific p27 using ELISA. Treatment with C-209 significantly reduced BMI-1 intratumor levels, while p27 intratumor levels were unchanged, confirming the specificity in BMI-1 targeting in primary and PCa grafts.

In **SUMMARY**, our recently published manuscript demonstrated that we have established a platform to utilize 1[ry] prostate in zebrafish (Bansal et al., Prostate) (in press, manuscript is attached in the appendix[2]) as biosensors to identify potent and selective BMI-1 inhibitors. We have examined a number of prostate cancer patients with adenocarcinomas and showed that BMI-1/CD44 correlate in high-grade histological and clinical prostate cancer.

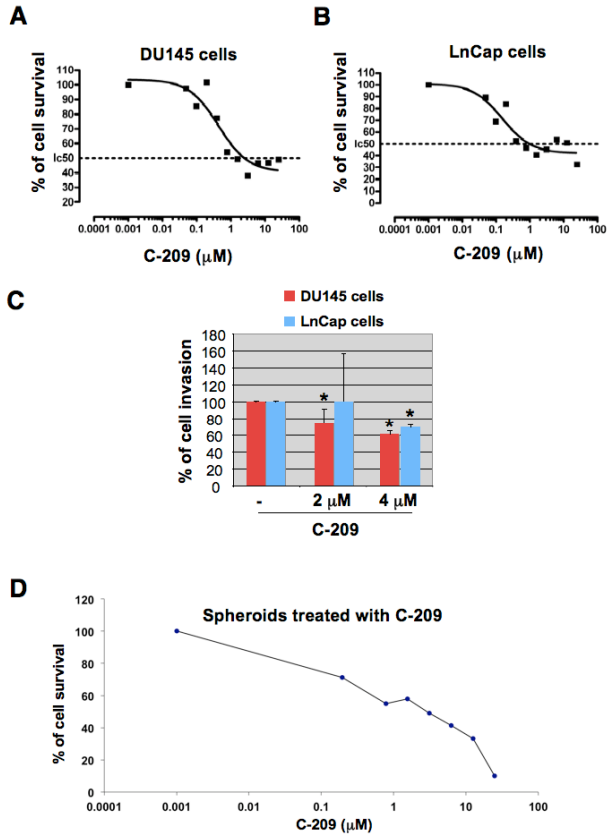

Figure 9. Comparing the antitumor activity of C-209 against DU145 and LnCap cells. **A-B,** DU145 and LnCap cells were treated with C-209 at different concentrations for 72hrs. MTS reagent was added to the cells and the color change was determined at OD of 490nm. Percentage of survival was calculated using PRIZM software. The IC_{50} of C-209 against DU145 and LnCap cells are approximately 2 μM and 1 μM, respectively. **C,** C-209 inhibits invasion of prostate cancer cells in matrigel. DU145and LnCap cells were treated with C-209, the cells were then plated on matrigel coated inserts for 24hrs. The inserts were then stained with crystal violet, and invaded cells were counted. Data are from three independent experiments done in triplicates for each treatment. **D,** Effect of C-209 on prostate spheroids with upregulated tumor stem cell markers. The spheroids formed from 5-min collagen attached cells were treated with C-209 at several concentrations (range 25 μM to 0.1μM) for 72hrs. The spheroids were then collected and replated in 96 well plates and MTS reagent was added. The absorbance was determined at OD 490nm, and data was analyzed using softmax pro software. IC_{50} of C-209 in spheroids formed from the 5-min collagen attached cells was determined to be ~3 uM.

We confirmed the activity of C-209 in zebrafish xenografts and further confirmed these findings in mouse prostate cancer xenografts. We will continue to study the roles of BMI-1 in regulating TICs in primary PCa[2], fish and mouse xenografts, and develop a defined rational for combination therapies during the second and third years of this project.

D. KEY RESEARCH ACCOMPLISHMENTS

- We developed a combined immunophenotypic and time-of-adherence assay to identify human prostate tumor initiating cells (TICs). These studies are recently accepted for publication and appeared in early online release on 24 Oct, 2013 (the full manuscript is attached in the appendix).

- We recruited 17 patients with prostate adenocarcinoma, and found increased BMI-1 and CD44 expression in cancer tissues compared to the adjacent normal tissues. These studies will continue with additional patients' tissues in the next year.

- Tumor initiation and dissemination were consistently observed in the immune-permissive zebrafish microenvironment from as-few-as 3 collagen-adherent $\alpha 2\beta 1^{hi}/CD44^{hi}$ cells.

- In zebrafish xenografts, self-renewing prostate TICs comprise 0.02-0.9% of PC3 cells, 0.3-1.3% of DU145 cells, and 0.22-25.0% of primary prostate adenocarcinomas.

- We uncovered a novel role for BMI-1 in metastasis based on data from zebrafish xenografts.

- Utilizing this zebrafish xenograft model, we identified the first known translational inhibitors of BMI-1 that target prostate TICs. The BMI-1 inhibitor C-209 induced prostate cancer cell senescence, and G1 cell cycle arrest.

- Targeting of BMI-1 with C-209 in prostate cancer significantly reduced clonogenic, migration, and invasion abilities of TICs, and increased cellular senescence.

- Treatment of zebrafish and mouse xenografts with the BMI-1 inhibitor C-209 reduced the metastatic potential of zebrafish TIC-derived xenografts, and inhibited tumor growth in mouse xenografts, respectively.

- These data support a paradigm of therapeutically targeting TICs in prostate cancer with C-209.

- The next stage will be the use of C-209 in combination therapy in zebrafish and mouse xenografts to develop a clinical strategy for the use of BMI-1 inhibitors in prostate cancer therapy.

E. REPORTABLE OUTCOMES

Manuscript:

Bansal N, Davis S, Tereshchenko I, Budak-Alpdogan T, Zhong H, Stein MN, Kim IY, DiPaola RS, Bertino JR, Sabaawy HE. Enrichment of human prostate cancer cells with tumor initiating properties in mouse and zebrafish xenografts by differential adhesion. Prostate. 2013 Oct 24. doi: 10.1002/pros.22740. [Epub ahead of print]. PMC: 24154958. (Full manuscript and supplemental data are attached in the appendix).

F. CONCLUSION

Prostate tumor-initiating cells (TICs) have intrinsic resistance to current therapies. BMI-1 (B-cell-specific MMLV insertion site-1) regulates stem cell self-renewal, and is over-expressed in TICs. We developed a combined immunophenotypic and time-of-adherence assay to identify human prostate TICs with increased BMI-1 expression. Tumor initiation and dissemination were consistently observed in the immune-permissive zebrafish microenvironment from as-few-as 3 collagen-adherent $\alpha2\beta1^{hi}/CD44^{hi}$ cells. In zebrafish xenografts, self-renewing prostate TICs comprise 0.02-0.9% of PC3 cells, 0.3-1.3% of DU145 cells, and 0.22-25.0% of primary prostate adenocarcinomas. Utilizing the zebrafish xenograft model, we identified the first known translational inhibitors of BMI-1 that target prostate TICs. BMI-1 inhibitors induced prostate cancer cell senescence, and G1 cell cycle arrest. Targeting of BMI-1 significantly reduced clonogenic, migration, and invasion abilities of TICs, and increased cellular senescence. Treatment of zebrafish and mouse xenografts with the BMI-1 inhibitor C-209 reduced the metastatic potential of zebrafish TIC-derived xenografts, and inhibited tumor growth in mouse xenografts, respectively. Therefore, we have accomplished our goal to demonstrate the beneficial effects of targeting prostate TICs with BMI-1 inhibitors during the first year of this project. This work also resulted in a publication demonstrating our ability to isolate and propagate primary prostate cancer TICs using the zebrafish xenograft assay. The next phase of studies will further examine the roles of BMI-1 targeted therapy in prostate cancer from additional primary tissues, and specifically examine the value of combining TICs-targeted therapy using BMI-1 inhibitors with common therapies targeting the bulk of prostate cancer such as Taxotere and other recently approved therapies in order to develop a therapeutic strategy for prostate cancer treatment by the completion of the project.

G. REFERENCES

1. Luo J, Zha S, Gage WR, Dunn TA, Hicks JL, Bennett CJ, Ewing CM, Platz EA, Ferdinandusse S, Wanders RJ, Trent JM, Isaacs WB, De Marzo AM. Alpha-methylacyl-CoA racemase: a new molecular marker for prostate cancer. Cancer Res 62:2220-6, (2002). PMC: 11956072.

2. Bansal N, Davis S, Tereshchenko I, Budak-Alpdogan T, Zhong H, Stein MN, Kim IY, DiPaola RS, Bertino JR, Sabaawy HE. Enrichment of human prostate cancer cells with tumor initiating properties in mouse and zebrafish xenografts by differential adhesion. Prostate, Oct 24. doi: 10.1002/pros.22740. [Epub ahead of print] (2013). PMC: 24154958.

3. Jin JK, Dayyani F, Gallick GE. Steps in prostate cancer progression that lead to bone metastasis. Int J Cancer 128:2545-61, (2011). PMC: 21365645.

4. Dayyani F, Gallick GE, Logothetis CJ, Corn PG. Novel therapies for metastatic castrate-resistant prostate cancer. J Natl Cancer Inst 103:1665-75, (2011). PMC: 21917607.

5. MacVicar GR, Hussain MH. Emerging therapies in metastatic castration-sensitive and castration-resistant prostate cancer. Curr Opin Oncol 25:252-60, (2013). PMC: 23511665.

6. Collins AT, Berry PA, Hyde C, Stower MJ, Maitland NJ. Prospective identification of tumorigenic prostate cancer stem cells. Cancer Res 65:10946-51, (2005). PMC: 16322242.

7. Guo C, Zhang B, Garraway IP. Isolation and characterization of human prostate stem/progenitor cells. Methods Mol Biol 879:315-26, (2012). PMC: 22610567.

8. Ramaswamy S, Ross KN, Lander ES, Golub TR. A molecular signature of metastasis in primary solid tumors. Nat Genet 33:49-54, (2003). PMC: 12469122.

9. Danila DC, Heller G, Gignac GA, Gonzalez-Espinoza R, Anand A, Tanaka E, Lilja H, Schwartz L, Larson S, Fleisher M, Scher HI. Circulating tumor cell number and prognosis in progressive castration-resistant prostate cancer. Clin Cancer Res 13:7053-8, (2007). PMC: 18056182.

10. Fan C, He L, Kapoor A, Gillis A, Rybak AP, Cutz JC, Tang D. Bmi1 promotes prostate tumorigenesis via inhibiting p16(INK4A) and p14(ARF) expression. Biochim Biophys Acta 1782:642-8, (2008). PMC: 18817867.

11. Fasano CA, Dimos JT, Ivanova NB, Lowry N, Lemischka IR, Temple S. shRNA knockdown of Bmi-1 reveals a critical role for p21-Rb pathway in NSC self-renewal during development. Cell Stem Cell 1:87-99, (2007). PMC: 18371338.

12. Song LB, Li J, Liao WT, Feng Y, Yu CP, Hu LJ, Kong QL, Xu LH, Zhang X, Liu WL, Li MZ, Zhang L, Kang TB, Fu LW, Huang WL, Xia YF, Tsao SW, Li M, Band V, Band H, Shi QH, Zeng YX, Zeng MS. The polycomb group protein Bmi-1 represses the tumor suppressor PTEN and induces epithelial-mesenchymal transition in human nasopharyngeal epithelial cells. J Clin Invest 119:3626-36, (2009). PMC: 19884659.

13. Dimri GP, Martinez JL, Jacobs JJ, Keblusek P, Itahana K, Van Lohuizen M, Campisi J, Wazer DE, Band V. The Bmi-1 oncogene induces telomerase activity and immortalizes human mammary epithelial cells. Cancer Res 62:4736-45, (2002). PMC: 12183433.

14. Liu S, Dontu G, Mantle ID, Patel S, Ahn NS, Jackson KW, Suri P, Wicha MS. Hedgehog signaling and Bmi-1 regulate self-renewal of normal and malignant human mammary stem cells. Cancer Res 66:6063-71, (2006). PMC: 16778178.

15. Jacobs JJ, Kieboom K, Marino S, DePinho RA, van Lohuizen M. The oncogene and Polycomb-group gene bmi-1 regulates cell proliferation and senescence through the ink4a locus. Nature 397:164-8, (1999). PMC: 9923679.

16. Cao Q, Mani RS, Ateeq B, Dhanasekaran SM, Asangani IA, Prensner JR, Kim JH, Brenner JC, Jing X, Cao X, Wang R, Li Y, Dahiya A, Wang L, Pandhi M, Lonigro RJ, Wu YM, Tomlins SA, Palanisamy N, Qin Z, Yu J, Maher CA, Varambally S, Chinnaiyan AM. Coordinated regulation of polycomb group complexes through microRNAs in cancer. Cancer Cell 20:187-99, (2011). PMC: 21840484.

17. Yang MH, Hsu DS, Wang HW, Wang HJ, Lan HY, Yang WH, Huang CH, Kao SY, Tzeng CH, Tai SK, Chang SY, Lee OK, Wu KJ. Bmi1 is essential in Twist1-induced epithelial-mesenchymal transition. Nat Cell Biol 12:982-92, (2010). PMC: 20818389.

18. Glinsky GV. Death-from-cancer signatures and stem cell contribution to metastatic cancer. Cell Cycle 4:1171-5, (2005). PMC: 16082216.

19. Berezovska OP, Glinskii AB, Yang Z, Li XM, Hoffman RM, Glinsky GV. Essential role for activation of the Polycomb group (PcG) protein chromatin silencing pathway in metastatic prostate cancer. Cell Cycle 5:1886-901, (2006). PMC: 16963837.

20. van Leenders GJ, Dukers D, Hessels D, van den Kieboom SW, Hulsbergen CA, Witjes JA, Otte AP, Meijer CJ, Raaphorst FM. Polycomb-group oncogenes EZH2, BMI1, and RING1 are overexpressed in prostate cancer with adverse pathologic and clinical features. Eur Urol 52:455-63, (2007). PMC: 17134822.

21. Cooper CS, Campbell C, Jhavar S. Mechanisms of Disease: biomarkers and molecular targets from microarray gene expression studies in prostate cancer. Nat Clin Pract Urol 4:677-87, (2007). PMC: 18059348.

22. Silva J, Garcia V, Garcia JM, Pena C, Dominguez G, Diaz R, Lorenzo Y, Hurtado A, Sanchez A, Bonilla F. Circulating Bmi-1 mRNA as a possible prognostic factor for advanced breast cancer patients. Breast Cancer Res 9:R55, (2007). PMC: 17711569.

23. Xu W, Zhou H, Qian H, Bu X, Chen D, Gu H, Zhu W, Yan Y, Mao F. Combination of circulating CXCR4 and Bmi-1 mRNA in plasma: A potential novel tumor marker for gastric cancer. Mol Med Rep 2:765-71, (2009). PMC: 21475899.

24. Zhang X, Wang C, Wang L, Du L, Wang S, Zheng G, Li W, Zhuang X, Dong Z. Detection of circulating Bmi-1 mRNA in plasma and its potential diagnostic and prognostic value for uterine cervical cancer. Int J Cancer 131:165-72, (2011). PMC: 21858805.

25. Tong YQ, Liu B, Zheng HY, He YJ, Gu J, Li F, Li Y. BMI-1 autoantibody as a new potential biomarker for cervical carcinoma. PLoS One 6:e27804, (2011). PMC: 22132147.

26. Siddique HR, Parray A, Zhong W, Karnes RJ, Bergstralh EJ, Koochekpour S, Rhim JS, Konety BR, Saleem M. BMI1, stem cell factor acting as novel serum-biomarker for Caucasian and African-American prostate cancer. PLoS One 8:e52993, (2013). PMC: 23308129.

27. Campbell PJ, Yachida S, Mudie LJ, Stephens PJ, Pleasance ED, Stebbings LA, Morsberger LA, Latimer C, McLaren S, Lin ML, McBride DJ, Varela I, Nik-Zainal SA, Leroy C, Jia M, Menzies A, Butler AP, Teague JW, Griffin CA, Burton J, Swerdlow H, Quail MA, Stratton MR, Iacobuzio-Donahue C, Futreal PA. The patterns and dynamics of genomic instability in metastatic pancreatic cancer. Nature 467:1109-13, (2010). PMC: 20981101.

28. Gerlinger M, Rowan AJ, Horswell S, Larkin J, Endesfelder D, Gronroos E, Martinez P, Matthews N, Stewart A, Tarpey P, Varela I, Phillimore B, Begum S, McDonald NQ, Butler A, Jones D, Raine K, Latimer C, Santos CR, Nohadani M, Eklund AC, Spencer-Dene B, Clark G, Pickering L, Stamp G, Gore M, Szallasi Z, Downward J, Futreal PA, Swanton C. Intratumor heterogeneity and branched evolution revealed by multiregion sequencing. N Engl J Med 366:883-92, (2012). PMC: 22397650.

29. Barbieri CE, Bangma CH, Bjartell A, Catto JW, Culig Z, Gronberg H, Luo J, Visakorpi T, Rubin MA. The mutational landscape of prostate cancer. Eur Urol 64:567-76, (2013). PMC: 23759327.

30. Magee JA, Piskounova E, Morrison SJ. Cancer stem cells: impact, heterogeneity, and uncertainty. Cancer Cell 21:283-96, (2012). PMC: 22439924.

31. Patrawala L, Calhoun T, Schneider-Broussard R, Li H, Bhatia B, Tang S, Reilly JG, Chandra D, Zhou J, Claypool K, Coghlan L, Tang DG. Highly purified CD44+ prostate cancer cells from xenograft human tumors are enriched in tumorigenic and metastatic progenitor cells. Oncogene 25:1696-708, (2006). PMC: 16449977.

32. Cao L, Bombard J, Cintron K, Sheedy J, Weetall ML, Davis TW. BMI1 as a novel target for drug discovery in cancer. J Cell Biochem, (2011). PMC: 21678481.

H. APPENDIX

Preprint of manuscript and supplemental data:

Bansal N, Davis S, Tereshchenko I, Budak-Alpdogan T, Zhong H, Stein MN, Kim IY, DiPaola RS, Bertino JR, Sabaawy HE. Enrichment of human prostate cancer cells with tumor initiating properties in mouse and zebrafish xenografts by differential adhesion. *Prostate*. 2013 Oct 24. doi: 10.1002/pros.22740. [Epub ahead of print]. PMC: 24154958.

Enrichment of Human Prostate Cancer Cells With Tumor Initiating Properties in Mouse and Zebrafish Xenografts by Differential Adhesion

Nitu Bansal,[1] Stephani Davis,[2] Irina Tereshchenko,[1] Tulin Budak-Alpdogan,[1] Hua Zhong,[3] Mark N. Stein,[1,4] Isaac Yi Kim,[1,5] Robert S. DiPaola,[1,4] Joseph R. Bertino,[1,2,4]* and Hatem E. Sabaawy[1,2,4]*

[1]*Rutgers Cancer Institute of New Jersey, New Brunswick, New Jersey*
[2]*Department of Pharmacology, Rutgers-Robert Wood Johnson Medical School, New Brunswick, New Jersey*
[3]*Department of Pathology and Laboratory Medicine, Rutgers-Robert Wood Johnson Medical School, New Brunswick, New Jersey*
[4]*Department of Medicine, Rutgers-Robert Wood Johnson Medical School, New Brunswick, New Jersey*
[5]*Department of Surgery, Rutgers-Robert Wood Johnson Medical School, New Brunswick, New Jersey*

BACKGROUND. Prostate tumor-initiating cells (TICs) have intrinsic resistance to current therapies. TICs are commonly isolated by cell sorting or dye exclusion, however, isolating TICs from limited primary prostate cancer (PCa) tissues is inherently inefficient. We adapted the collagen adherence feature to develop a combined immunophenotypic and time-of-adherence assay to identify human prostate TICs.

METHODS. PCa cells from multiple cell lines and primary tissues were allowed to adhere to several matrix molecules, and fractions of adherent cells were examined for their TIC properties.

RESULTS. Collagen I rapidly-adherent PCa cells have significantly higher clonogenic, migration, and invasion abilities, and initiated more tumor xenografts in mice when compared to slowly-adherent and no-adherent cells. To determine the relative frequency of TICs among PCa cell lines and primary PCa cells, we utilized zebrafish xenografts to define the tumor initiation potential of serial dilutions of rapidly-adherent $\alpha2\beta1^{hi}/CD44^{hi}$ cells compared to non-adherent cells with $\alpha2\beta1^{low}/CD44^{low}$ phenotype. Tumor initiation from rapidly-adherent $\alpha2\beta1^{hi}/CD44^{hi}$ TICs harboring the TMPRSS2:ERG fusion generated xenografts comprising of PCa cells expressing Erg, AMACR, and PSA. Moreover, PCa-cell dissemination was consistently observed in the immune-permissive zebrafish microenvironment from as-few-as 3 rapidly-adherent $\alpha2\beta1^{hi}/CD44^{hi}$ cells. In zebrafish xenografts, self-renewing prostate TICs

Grant sponsor: Department of Defense Prostate Cancer Grants; Grant number: W81XWH-12-1-0251; Grant sponsor: Rutgers Cancer Institute of New Jersey (Pilot Grant).

Authors Contributions: 1. Conception and design—Nitu Bansal, Hatem E. Sabaawy, Joseph R. Bertino. 2. Provision of study material or patient samples—Mark N. Stein, Hua Zhong, Isaac Yi Kim. 3. Collection and assembly of data—Nitu Bansal, Stephani Davis, Hatem E. Sabaawy. 4. Data analyses—Nitu Bansal, Irina Tereshchenko, Hatem E. Sabaawy, Robert DiPaola, Joseph R. Bertino. 5. Manuscript writing—Hatem E. Sabaawy, Joseph R. Bertino.

All authors declare no competing interest.

*Correspondence to: Joseph R. Bertino, MD, Rutgers Cancer Institute of New Jersey, 195 Little Albany Street, Room 3033, New Brunswick, NJ 08903-2681. E-mail: Joseph.Bertino@rutgers.edu

**Correspondence to: Hatem E. Sabaawy, MD, PhD, Rutgers Cancer Institute of New Jersey, 195 Little Albany Street, Room 4557, New Brunswick, NJ 08903-2681. E-mail: Hatem.Sabaawy@rutgers.edu

Received 2 May 2013; Accepted 15 September 2013
DOI 10.1002/pros.22740
Published online in Wiley Online Library
(wileyonlinelibrary.com).

comprise 0.02–0.9% of PC3 cells, 0.3–1.3% of DU145 cells, and 0.22–14.3% of primary prostate adenocarcinomas.

CONCLUSION. Zebrafish PCa xenografts were used to determine that the frequency of prostate TICs varies among PCa cell lines and primary PCa tissues. These data support a paradigm of utilizing zebrafish xenografts to evaluate novel therapies targeting TICs in prostate cancer. *Prostate* © 2013 Wiley Periodicals, Inc.

KEY WORDS: **prostate cancer stem cells; tumor-initiating cells; zebrafish**

INTRODUCTION

Prostate cancers (PCa) were suggested to contain tumor cells that can self-renew, differentiate into multiple cell types reconstituting the diverse tumor population, and have enhanced proliferative capacity to drive the continued expansion of malignant cells [1]. These cells were identified as tumor-initiating cells (TICs) [2,3] that are able to form tumors in immune-compromised mice, and self-renew in serial transplantation studies [4]. Genetic and lineage tracing studies have recently provided substantial evidence that subpopulations of tumor cells or TICs direct tumor growth in mice [5–7]. These cells survive treatments by virtue of possessing anti-apoptotic signals, high levels of drug-efflux membrane transporters, and high DNA repair capacity [8]. Since TICs are commonly resistant to conventional chemotherapies, and prostate tumors develop resistance to hormonal ablation therapy [9], an attractive cancer treatment strategy is to identify TICs and then use agents that effectively target the self-renewal abilities of TICs, alone or in combination with hormone ablation as an initial therapy to accomplish total tumor eradication, and to reduce the risk of relapse and metastasis.

PCa TICs showed enhanced expression of self-renewal and stem cell markers such as Bmi-1, Oct4, β-catenin, and SMO supporting the presence of prostate TICs with stem cell properties [10]. Moreover, knockdown of these self-renewal signals in metastatic PCa leads to tumor cell death [11]. Thus, development of methods to enrich for TICs would provide a platform for the identification and preclinical examination of novel therapies that target self-renewal signals in prostate TICs.

Prostate tumors contain several functionally diverse cell types including TICs that can be of basal and/or luminal origin(s) [12], transit amplifying cells, terminally differentiated cells, and supportive stromal cells. The fraction of cells with TIC abilities would likely vary among different PCa cell lines and primary patient samples; however, it is generally believed to be a smaller fraction of cells within each tumor. Therefore, isolating the TIC subpopulation from a limited number of fresh primary PCa cells for study and manipulation is inherently inefficient.

PCa cells were shown to harbor a series of TMPRSS2-Ets fusion proteins generated through chromosomal translocations [13], and detected using interphase fluorescent in situ hybridization (FISH) techniques. The TMPRSS2-Ets fusions frequently result in overexpression of Ets proteins such as Erg when PCa cells are examined with immunohistochemistry (IHC), making overexpression of Erg as one of the most PCa-specific biomarkers yet identified [14]. Another biomarker is the overexpression of alpha-methylacyl coenzyme A racemase (AMACR), which in combination with absence of basal cell layer markers are typical phenotypes of acinar prostatic adenocarcinoma. Integrin-β-1 has also been recognized as a basal cell marker associated with certain stem cell properties, and has been used as a cell surface maker for enrichment of epidermal keratinocyte stem cells [15] and human prostate epithelial stem cells [16]. We attempted to enrich putative TICs from PCa cell lines and primary samples based on adhesion to collagen I, collagen VI, or laminin; that are all β1-Integrin ligands. We then examined their TIC properties in vitro and in vivo in mice and zebrafish xenografts.

Tumor cell xenografts in the teleost zebrafish (*Danio rerio*) might allow for monitoring of tumor initiation from a limited number of TICs, thus mimicking the orderly stages of tumor growth, relapse, and metastasis. The zebrafish xenograft model offers several advantages over traditional murine and chick embryo xenograft models. Zebrafish embryos are small, develop rapidly, and hundreds are produced daily from each pair, making zebrafish an excellent vertebrate tool for testing chemicals in vivo, and for cancer drug discovery [17]. The optical clarity of zebrafish embryos and Casper [18] adult fish allows for non-invasive observation of tumor initiation, migration, and metastasis [19–21]. Earlier TIC reports suggested that TICs from the same patient are more prevalent in the highly immune-permissive NOD-SCID-IL2Rγ deficient mice than in the NOD-SCID deficient mice [22]. In contrast, the use of zebrafish embryos in a pre-immune, more xenograft-tolerant,

environment would be advantageous to determine the self-renewal potential of prostate TICs.

Here, we demonstrate that a fraction of cells isolated from multiple PCa cell lines and primary cells have tumor initiation potential in mice and zebrafish. Moreover, we found that prostate TIC frequency of primary PCa cells is much higher than TIC frequency of cells from established PCa cell lines in zebrafish xenografts.

MATERIALS AND METHODS

Materials

Taxotere, doxorubicin, and methotrexate were from the Cancer Institute of New Jersey pharmacy. Both collagen I, IV and laminin were purchased from BD Biosciences, and athymic$^{nu/nu}$ mice were from Jackson laboratory.

Fresh Human Prostate Cancer Samples

PCa patients diagnosed at the CINJ between 2008 and 2012 were enrolled. Prostate TICs and populations lacking TICs were isolated and characterized from prostatectomy specimens. Informed consents were obtained. De-identified PCa specimens were collected under institutional review board (IRB)-approved protocol. We used samples with similar Gleason scores determined through the review of diagnostic pathology reports. Primary cells were isolated as described in supplementary methods, allowed to adhere to collagen I, and subfractions were sorted and transplanted into fish embryos.

Cell Lines Culture, Prostate Spheres, Colony Formation, Migration, and Invasion Assays

Prostate normal and cancer cells were maintained at low passage numbers and utilized for clonogenic, migration, invasion, and prostate sphere forming assays as described in supplementary methods and elsewhere [23–25].

Collagen Adherence Assay

Putative TICs were isolated by combining phenotypic analyses [3] with collagen I adherence. In brief, tissue culture dishes were coated with 70 μg/ml of collagen I for 1 hr at room temperature or overnight at 4°C. Plates were washed with PBS, blocked in 0.3% BSA for 30 min, washed again, and cells were plated on collagen I for 5 or 20 min. Cells that adhere in 5 min, and cells that did not adhere after 20 min were collected, and used.

Flow Cytometry, IHC, Interphase FISH, and Cytotoxicity Assays

Prostate cells were analyzed using FACScan cytometer and CellQuest software (BD). Flow cytometry, IHC, interphase FISH for TMPRSS2:Erg fusions, and cytotoxicity assays were performed as described in supplementary methods. IC_{50} concentrations used in cytotoxicity assays are described in supplementary methods and Supplementary Figure S1D, and were determined using Hill's equation in Graph-Pad prism 4.0 software.

Xenograft Studies in Nude Mice

Animals were used in accordance with an approved protocol from RWJMS. PCa cells, 5 min collagen adherent, and 20 min non-adherent cells were injected along with matrigel in a 1:1 ratio into the abdominal flanks of nude mice ($n = 8$ mice/group). A subset of each cell population was analyzed for cell viability to confirm that viable cells were being injected into the mice. Every 3 days, tumor dimensions were measured using a Vernier caliper, and tumor volumes were calculated as described [26].

Labeling and Transplantation of Prostate Cancer Cells in Zebrafish

Wild type EKK and AB* zebrafish (*D. rerio*) were maintained following an approved animal protocol. Adult fish were spawned and reared in conditioned water at 28.5°C on a 14-hr light–10-hr dark cycle. Embryos were staged as described (http://zfin.org). To track human cells in embryos and juvenile Casper [18] fish, we labeled PCa cells with quantum dots (QDs) that are virtually resistant to photobleaching. PCa cells were resuspended in 0.5× Dulbecco's PBS (DPBS) containing QD605 (red fluorescence; Invitrogen) and lipofectamine at a ratio of 1:2 for 2 hr. Cells in 0.5× DPBS were used for transplantation into dechorionated and anesthetized (0.5× tricaine methanesulfonate, MS-222; Sigma) 48-hr post-fertilization (hpf) embryos using 15 μm (internal diameter) injection needles. Transplantation of fresh cells or cells dissociated from primary xenograft regions and sorted for serial transplantation were done as described in supplementary methods and as previously described [27]. Microinjections were either subcutaneously (SC), or above the yolk into the sinus venosus using a Celltram microinjector. After transplantation and initial imaging, embryos were incubated for 2 hr at 37°C, and were then maintained in a humidified incubator at 33–34°C for up to 12 days post-transplantation (dpt). Human cells were monitored under fluorescent microscopy for homing and

tissue repopulation. Juvenile zebrafish at 6–8 weeks of age were immune-suppressed with 10 μg/ml dexamethazone for 2 days as previously described [19,28], and were also utilized to generate xenografts. Juvenile fish were monitored for tumor growth and metastasis for up to 5 weeks.

Extreme Limiting Dilution Analysis (ELDA)

ELDA was used to assess the number of self-renewing cells contained within the bulk of the primary PCa mass as described in supplementary methods. The TIC frequency was finally calculated after 12 dpt using a linear regression method that was completed using ELDA [29] at http://bioinf.wehi.edu.au/cgi-bin/limdil/limdil.pl.

Statistical Analysis

All experiments were performed thrice, and each experiment was done in triplicates. Statistical analyses were done using Student's *t*-test unless otherwise indicated. Results are presented as mean ± standard deviation (SD). Limiting dilution analysis (LDA), ELDA [29], and L-Calc statistical software were used to determine the frequencies of self-renewing TICs. A *P*-value of <0.05 was considered significant.

RESULTS

Isolation and Characterization of Human Prostate Tumor-Initiating Cells

Several strategies have been proposed to isolate prostate TICs, including the use of a combination of unique surface markers. Phenotypic markers identified for prostate TICs are $CD44^{hi}$, $CD44^{+}/CD24^{-}$ [30], and $CD44^{hi}$, α2β1-$integrin^{hi}$, and $CD133^{+}$ [3,16]. Trop2 marker has also been used in combination with $CD49f^{+}$ to enrich for sphere-forming cells from human prostate [31]. We elected to use a strategy of combining phenotypic and time-of-adherence assays to isolate TICs from PCa cells. The adhesion properties of PCa cells were examined by incubating cells on either laminin-, collagen I-, collagen IV-coated dishes, or when all three matrix molecules are combined for different lengths of time from 5, 10, 15, to 20 min. As seen in Figure 1 for DU145 cells from six separate adhesion experiments, PCa cells rapidly adhered to collagen I-coated dishes within 5 min. The assay is based on the finding that epidermal and testicular stem cells express higher levels of α2β1- and α3β1-integrins than transit amplifying or differentiated cells [32,33]. To isolate putative TICs, PCa cells from four cell lines and six primary patient prostatectomies

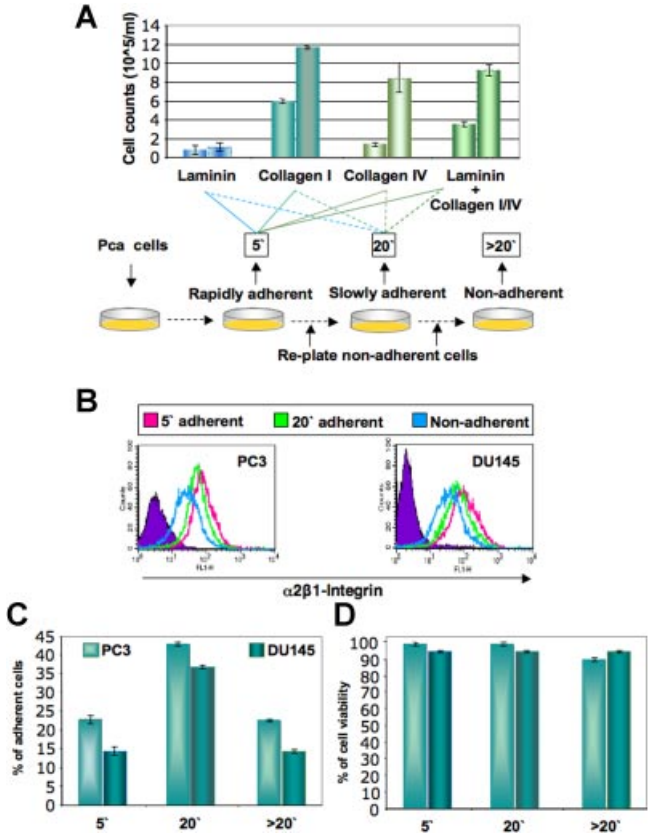

Fig. 1. Isolation of subpopulations of prostate cancer cells by differential adherence. **A**: Multiple prostate cancer cell lines were allowed to adhere to either laminin-, collagen I-, collagen IV-coated plates, or plates coated with all three combinations. Time of adherence assay is described where PCa cells are allowed to adhere for 5 min, the rapidly adherent cells after 5 min (5′) are collected, the remaining of the cells are replated for 20 min, the cells that adhere at 20 min (20′) are collected, and the cells that did not adhere (>20′ are labeled as non-adherent cells. Data are shown for DU145 cells from six separate adhesion experiments. **B**: Fractions of PC3 and DU145 cells collected after time-of-adherence assay were subjected to flow cytometric analysis of α2β1-integrin expression. Representative flow cytometric analysis is shown for PC3 and DU145 cells. **C**: Percentages of collagen I adherent and non-adherent PC3 and DU145 cells immediately after collagen adherence assay. **D**: Cell viability of collagen I adherent and non-adherent PC3 and DU145 cells immediately after the collagen adherence assay were similar to cell viabilities of adherent and non-adherent cells immediately after cell isolation, and averaged 95–99.9%.

(Table I) were plated on collagen I-coated dishes for 5 min, and adherent cells were collected. Non-adherent cells were replated for 20 min. After 20 min, non-adherent cells were also collected. To investigate whether the rapidly collagen-adherent cells (at 5 min) had increased expression of α2β1-integrin positive cells (a marker for TICs), we performed flow cytometric analyses of the different fractions, and found that

TABLE I. TIC Frequencies of Cells From Primary Prostate Cancer Patients in Zebrafish Xenografts

1^{ry} prostate	Gleason	R^2	99% confidence	TIC frequency
1	3 + 3	0.999	1/7–1/37	1/16
2	3 + 3	0.995	1/29–1/153	1/71
3	3 + 3	0.995	1/64–1/228	1/120
4	3 + 3	0.999	1/59–1/456	1/185
5	3 + 3	0.995	1/32–1/114	1/36
6	3 + 4	0.998	1/29–1/153	1/71

Table shows patient number and Gleason scores. TIC frequencies of 1/16 (6.25%), 1/71 (1.4%), 1/120 (0.83%), 1/185 (0.54%), 1/36 (2.7%), 1/71 (1.4%), 1/8 (12.5%), 1/16 (6.25%), and a frequency range of 0.22–25.0% were calculated in the six patient samples using ELDA with 99% confidence interval, and with the displayed correlation coefficient (R^2) values. Fifty embryos per dilution per tumor sample were transplanted SC with limiting dilution (3–100 cells) of TICs from the 5 min adherent $\alpha2\beta1^{hi}$/$CD44^{hi}$ cells. Tumor cell graft take was consistently high, and averaged 77 ± 10%, and embryo survival next day after transplantation was >86%.

the rapidly adherent cells have higher α2β1-integrin expression from both DU145 and PC3 cells (Fig. 1B) compared to the 20 min non-adherent cells. Differential adhesion was readily detectable when collagen I was used (Fig. 1A), hence we performed further experiments utilizing collagen I. Similar percentages of collagen I adherent cells were seen from both DU145 and PC3 cells (Fig. 1C). To exclude that the differential adhesion of PCa cells to collagen I-coated dishes was due to differences in cell viability or interference with cell proliferation abilities, we compared the proliferation of the differentially adherent fractions to the non-selected ones, and found no significant difference in cell proliferation (Supplementary Fig. S1). Cell viabilities of adherent and non-adherent cells immediately after cell isolation were similar (Fig. 1D) and were on average 95–99.9%. We also found that the rapidly adherent cells retained a more cohesive colony-like morphology after plating for 6 days, while 20 min non-adherent and adherent cells retained a less cohesive and mixed morphology, respectively (Supplementary Fig. S1).

We then examined the expression of stem cell markers in DU145, PC3, LNCap, and CWR22 PCa cells. $CD44^{hi}$ and α2β1-$integrin^{hi}$ cells were detected in all four cell lines (Fig. 2A), while CD133 expression was very low (≤0.01%) to not detectable. We isolated TICs from these PCa cell lines by combining phenotypic selection with collagen I adherence. The 5 min adherent cell fraction comprised on average 4–6% of DU145 and PC3 cells, but was two- to threefold less in both LNCap and CWR22 cells (Fig. 2B). Expression of CD44, α2β1-integrin, and CD133 in each fraction was analyzed. The 5 min adherent cell fraction had an average of several fold higher number of cells highly coexpressing α2β1 and CD44 as compared to the 20 min non-adherent fractions in all of the PCa cells examined (Fig. 2B and Supplementary Fig. S2A). Thus phenotypically, the 5 min adherent fraction is enriched in $\alpha2\beta1^{hi}$/$CD44^{hi}$ cells, while the 20 min non-adherent fraction comprise $\alpha2\beta1^{low}$/$CD44^{low}$ cells. When cells from the 5 min adherent fraction of PC3 and DU145 cells that are $\alpha2\beta1^{hi}$/$CD44^{hi}$ cells were grown as prostate spheres, known to contain putative TICs that can initiate serially passageable spheres, the consistently low CD133 expression increased, and up to 5% of the cells were $CD133^{+}$ (Fig. 2D). Significant upregulation of CD133 expression was detected in spheres of DU145 and PC3 cells (Fig. 2D) and CWR22 cells (Supplementary Fig. S2C), while CD133 was still undetectable in LNCap cells when grown as prostate spheres.

To examine if combining phenotypic and time-of-adherence assays could be used to isolate TICs from primary PCa cases (n = 6), we collected fresh tissues from 6 matched PCa patients with similar Gleason scores (Table I), and subjected them to the same assay. Similar to PCa cell lines, the 5 min adherent fraction from primary samples was enriched in $\alpha2\beta1^{hi}$/$CD44^{hi}$ cells, and in $CD133^{+}$ cells when grown as prostate spheres, compared to the non-adherent fraction (Fig. 2E).

Tumorigenic and Self-Renewal Capacities of Adherent Tumor Cells

To determine if the 5 min adherent cell fraction contains TICs, $\alpha2\beta1^{hi}$/$CD44^{hi}$ DU145 cells within this fraction were examined by colony formation, and migration and invasion assays. The 5 min adherent cell fraction with an $\alpha2\beta1^{hi}$/$CD44^{hi}$ phenotype showed a nearly twofold higher colony formation (Fig. 3A), and increased migration and invasion abilities as compared to $\alpha2\beta1^{low}$/$CD44^{low}$ cells (Fig. 3A). Similarly, PC3, CWR22, and LNCap cells within the 5 min adherent cell fractions with an $\alpha2\beta1^{hi}$/$CD44^{hi}$ phenotype showed variable but consistently higher colony and spheroid formation abilities (Supplementary Fig. S2A–C). Since DU145 and PC3 cells displayed a larger 5 min adherent cell fraction with an $\alpha2\beta1^{hi}$/$CD44^{hi}$ phenotype, we utilized these cells in most of our assays. An essential characteristic of TICs is their ability to self-renew in serial plating assays. The $\alpha2\beta1^{hi}$/$CD44^{hi}$ DU145 cells formed significantly more single cell-derived spheroids as compared to $\alpha2\beta1^{low}$/$CD44^{low}$ cells. Moreover, spheroids formed from

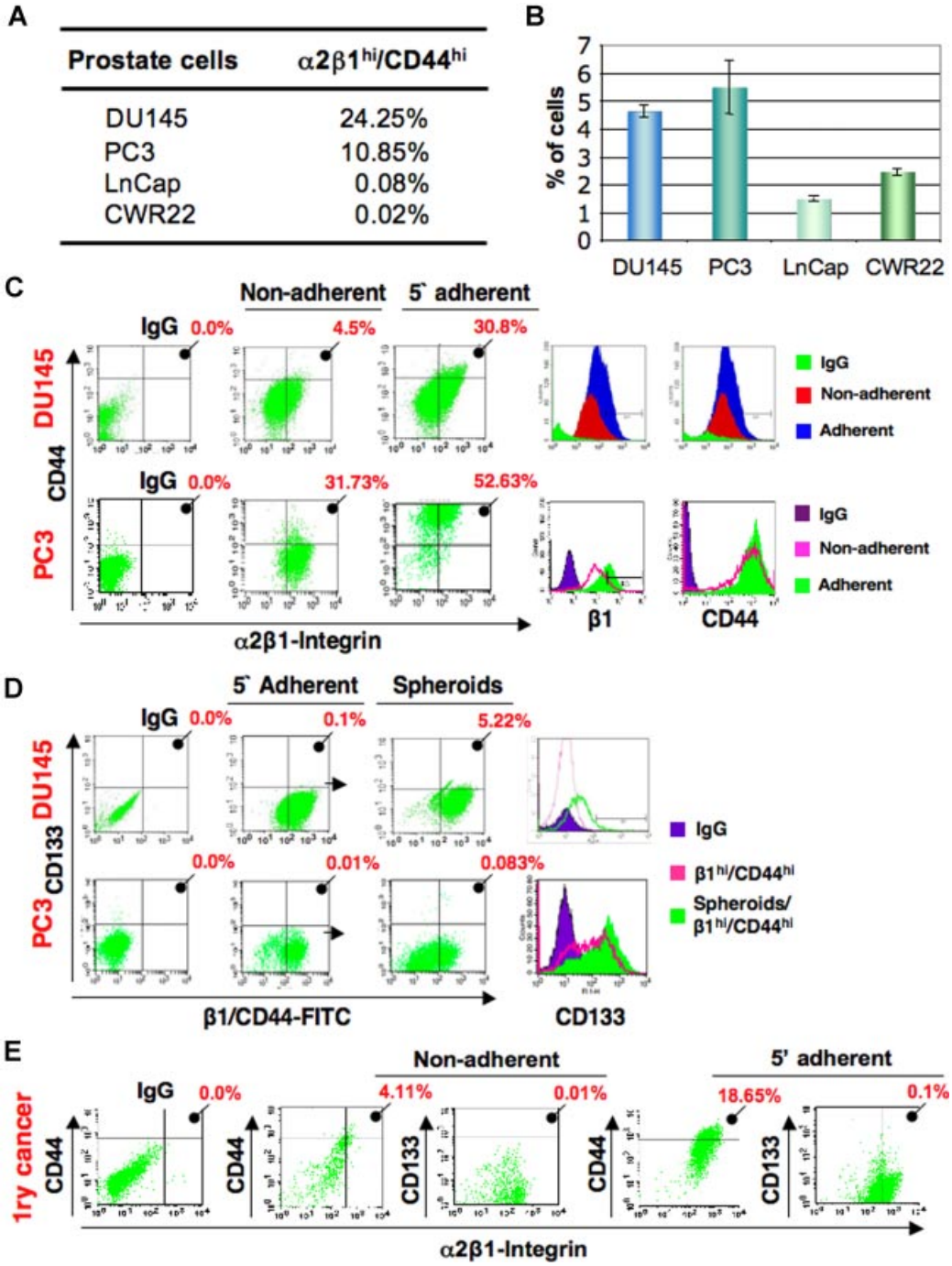

Fig. 2. Collagen-adherent cells are enriched in putative TICs. **A**: Mean percentage of cells with $\alpha 2\beta 1^{hi}/CD44^{hi}$ phenotype in PCa cell lines. **B**: Time-of-adherence assay performed on multiple PCa cell lines displaying the 5 min adherent cell fraction as a percentage of total cells. Data represent three independent experiments performed in triplicates. **C**: Flow cytometric analyses of DU145 and PC3 cells after collagen adherence showing both increased expression of CD44 and CD133 in the 5 min (5′) adherent cells compared to the 20 min (20′) non-adherent cells, and higher mean fluorescence intensity (MFI) of 5 min collagen I-adherent ($\alpha 2\beta 1^{hi}/CD44^{hi}$) cells (Adherent) compared to 20 min non-adherent ($\alpha 2\beta 1^{low}/CD44^{low}$) cells (Non-adherent), and IgG control (IgG). **D**: CD133 expression in various subsets of DU145 and PC3 cells. In a representative experiment, $\alpha 2\beta 1^{hi}/CD44^{hi}$ (pink) showed 0.1% and 0.01% of the cells positive for CD133 from DU145 and PC3 cells respectively, and spheroids from these $\alpha 2\beta 1^{hi}/CD44^{hi}$ cells (green) showed upregulated CD133 levels up to 5.22% in DU145 cells and 0.083% in PC3 cells ($P < 0.001$ for both cell lines in three independent experiments). **E**: Primary prostate cancer cells have increased expression of CD44 and CD133 in the 5 min adherent cells compared to the 20 min non-adherent cells. Mean percentages from analyses of six cases are displayed. Higher expression of $\alpha 2\beta 1$/CD44 and upregulation of CD133 when cells are grown as spheres were detected in the 5 min adherent cells compared to the 20 min non-adherent cells, and were seen with all six patient samples examined.

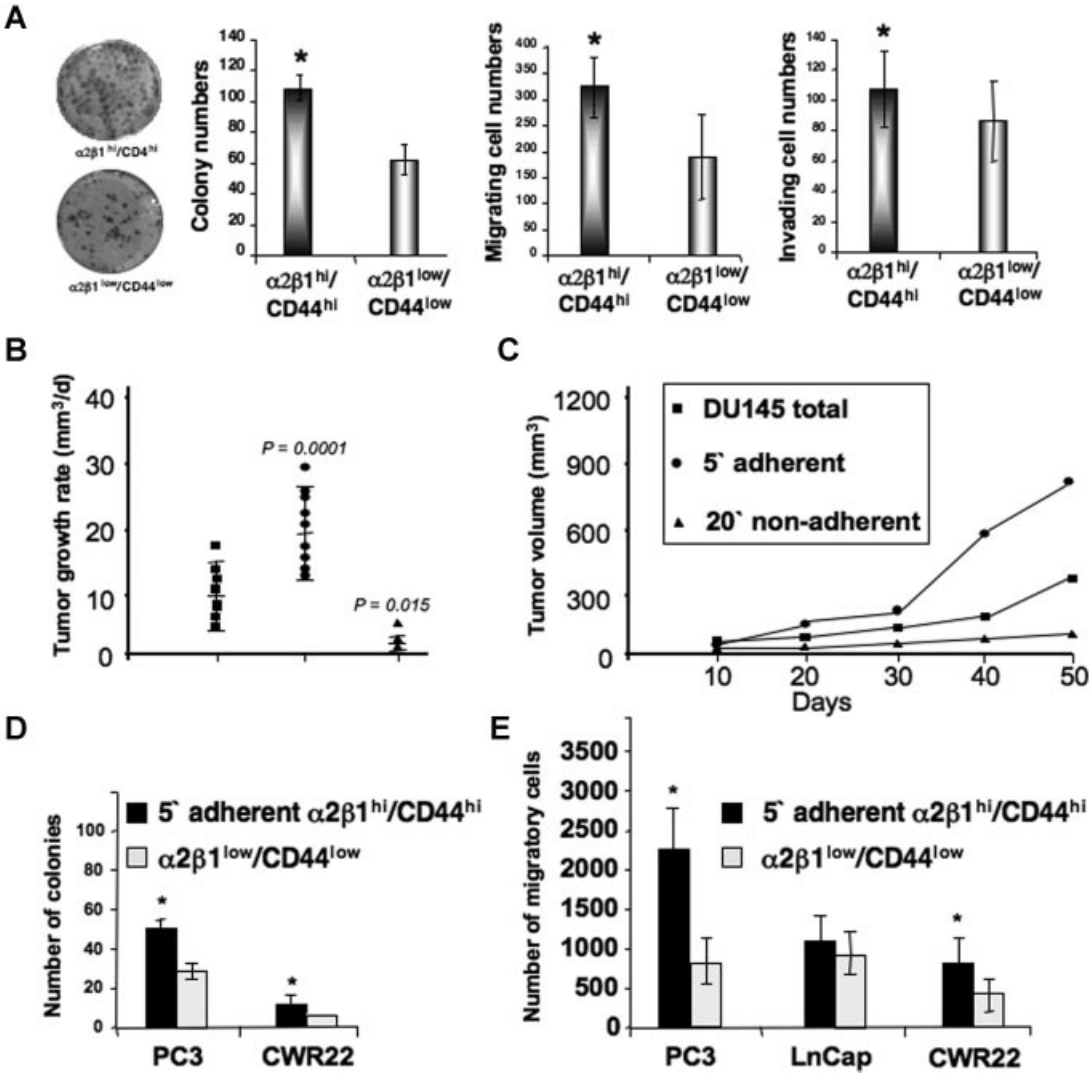

Fig. 3. Tumorigenic potential of collagen-adherent $\alpha2\beta1^{hi}/CD44^{hi}$ cells. **A**: The two fractions of $\alpha2\beta1^{hi}/CD44^{hi}$ cells and $\alpha2\beta1^{low}/CD44^{low}$ cells isolated after collagen adherence were assessed in colony forming efficiency assays. Images on the left demonstrate colonies derived from both fractions stained with crystal violet. Numbers of spheroid colonies, migrating, and invading cells are displayed as mean ± SD, and were done in triplicates. Self-renewal and in vitro tumorigenic potential of collagen-adherent $\alpha2\beta1^{hi}/CD44^{hi}$ DU145 cells are shown. Bars demonstrate the enhanced clonogenic ability of $\alpha2\beta1^{hi}/CD44^{hi}$ cells compared to $\alpha2\beta1^{low}/CD44^{low}$ cells. The two fractions of $\alpha2\beta1^{hi}/CD44^{hi}$ cells and $\alpha2\beta1^{low}/CD44^{low}$ DU145 cells isolated after collagen adherence were assessed for numbers of migrating cells. Data are displayed as mean ± SD, and were done in triplicates ($^*P < 0.001$). **B**: Both flanks of athymic nude ($NCI^{nu/nu}$) mice were injected with either total DU145 cells (■), 5 min adherent cells (●), or 20 min non-adherent cells (▲) (n = 60 mice). Mean tumor growth rates are presented as mm^3/day ± SD. **C**: The mean tumor volume was plotted as a function of time using the ellipsoid volume formula (length × width^2 × 1/2), assuming $\pi = 3$. *P* values shown are compared with total DU145 tumors. **D**,**E**: Self-renewal and in vitro tumorigenic potential of collagen-adherent $\alpha2\beta1^{hi}/CD44^{hi}$ PC3, LnCap and CWR22 PCa cells. D: Bars demonstrate the enhanced clonogenic ability of $\alpha2\beta1^{hi}/CD44^{hi}$ cells compared to $\alpha2\beta1^{low}/CD44^{low}$ PC3 and CWR22 cells. E: The two fractions of $\alpha2\beta1^{hi}/CD44^{hi}$ cells and $\alpha2\beta1^{low}/CD44^{low}$ PC3, LnCap and CWR22 cells isolated after collagen adherence were assessed for numbers of migrating cells. Data are displayed as mean ± SD, and were done in triplicates ($^*P < 0.001$).

$\alpha2\beta1^{low}/CD44^{low}$ DU145 cells were fewer after day 5, and stopped growing after day 9 (Supplementary Fig. S3A and B) suggesting that these cells lack self-renewal abilities. To assess self-renewal at an earlier time point of sphere formation, single cells derived from day 7-primary spheroids were replated for secondary spheroid formation. Once again, $\alpha2\beta1^{hi}/CD44^{hi}$ DU145 cells generated significantly more spheroids than $\alpha2\beta1^{low}/CD44^{low}$ cells (Supplementary Fig. S3C). Therefore, the $\alpha2\beta1^{hi}/CD44^{hi}$ PCa cells exhibit enhanced tumorigenic, invasive, and self-renewal abilities.

Adherent Cells Are Resistant to Commonly Used Chemotherapeutic Drugs

Breast TICs were shown to be resistant to chemotherapies [34]. Since we isolated putative prostate TICs by collagen adherence, we hypothesized that treatment with drugs that target TICs would reduce the number of cells adhering to collagen I. Hence, we performed the collagen adherence assay upon treatment with chemotherapies commonly used for PCa at IC_{50s} established by MTS assays (Supplementary Fig. S3D). Indeed, the number of DU145 collagen-adherent cells was not affected by chemotherapy treatments, and on the contrary increased with methotrexate and carboplatin (Supplementary Fig. S3E) suggesting that these mainstream clinically used chemotherapeutic agents might increase the percentage of putative TICs.

Tumor Initiation in Nude Mice

An essential property of TICs is their ability to initiate tumor growth in immune-compromised mice with limited cell numbers. We tested whether the 5 min adherent DU145 cells are more tumorigenic than the non-adherent fraction. Cells were injected SC in the abdominal flanks of nude mice. Tumors were analyzed by three variables: tumor incidence, tumor growth rate (mm^3/day), and final tumor volume (mm^3; Fig. 3B and C). Only 17% of mice (n = 3/20) injected with non-adherent cells developed tumors, while nearly all mice injected with either adherent (n = 18/20; 90%) or total DU145 cells (n = 17/20; 85%) developed tumors. Mice injected with adherent cells developed tumors as early as 15 days post-transplantation, compared to day 35 for mice injected with the same cell dose of one million total DU145 cells. In an additional experiment, injection of only 1,000 adherent cells resulted in tumor formation and tumor volumes that were significantly larger than those generated by injections of one million total DU145 cells (data not shown). After 50 days of growth, adherent DU145 tumors reached an average final volume of 867 mm^3. This was significantly larger than non-adherent and total DU145 tumors (Fig. 3B and C), which reached final volumes of 126 and 338 mm^3, with P values of 0.0006 and 0.0001, respectively when compared with adherent cell tumors. Thus, the adherent $\alpha2\beta1^{hi}$/$CD44^{hi}$ DU145 cells are more tumorigenic in mice.

Evaluation of Prostate TICs In Vivo in Zebrafish Xenografts

To generate a PCa xenograft model in zebrafish for studying TICs, we employed a collagen adherence, cell sorting, and QD labeling strategy. Cells from PCa cell lines and primary samples were QD labeled at near-100% efficiency (Fig. 4A and B). QD-labeled PCa cells, but not normal prostate epithelial cells, engrafted robustly in the pre-immune zebrafish embryos, and histological analyses demonstrated cells migrating to distal sites in zebrafish including muscle regions (Fig. 4C and D). Embryos with xenografts from the 5 min adherent $\alpha2\beta1^{hi}$/$CD44^{hi}$ PCa cells displayed significantly shorter survival rates, and rapid death from tumor burden with a median survival of 100 ± 19 hr post-transplant (hpt), compared to median survivals of 108 ± 10 hpt and 186 ± 23 hpt for the parental DU145 and the $\alpha2\beta1^{low}$/$CD44^{low}$ cells, respectively (Fig. 4E) (n = 200 embryo/group, $P < 0.001$). Similar data were obtained from PC3, CWR22 and LNCap cells (Fig. 4E) as well as primary PCa cells (see below). The maximum tolerated cell doses for DU145, PC3, and primary PCa cell transplants ranged from 0.4 to 2×10^3 cells, which resulted in death from generalized tumor burden at 2–5 dpt with PCa cells but not with immortalized normal prostate epithelial cells (RWPE-1) (Fig. 4E). QD-labeled parental cells, $\alpha2\beta1^{hi}$/$CD44^{hi}$ cells sorted from 5 min adherent cells, and $\alpha2\beta1^{low}$/$CD44^{low}$ cells sorted from 20 min non-adherent cells were transplanted at limiting dilution with cell doses from 1×10^3 to 3 cells either SC to allow for tumor cell dissemination or into the yolk of 48-hpf zebrafish embryos. We sorted embryos post-injection to ensure the placement and number of labeled cells, and grew the selected embryos at 33°C.

Transplanted cells and tumor growth were traceable in vivo in living fish (Fig. 5A). QD-labeled primary PCa cells (Fig. 5A) or DU145 cells (Fig. 5B–E) developed xenografts in zebrafish embryos. DU145 cells injected SC formed localized tumor xenografts at 4 dpt (Fig. 5B) that frequently migrated throughout the zebrafish muscle tissues, and often spread causing brain metastasis (Fig. 5D and E, left arrow), exophthalmus (Fig. 5D, arrowheads; Supplementary Table SI), and death from disseminated tumor burden within 9 dpt. Cells in xenografts derived from adherent $\alpha2\beta1^{hi}$/$CD44^{hi}$ (TICs) disseminated to the brain region of zebrafish embryos, and were detected using IHC with the human-specific CD44 isoform (Fig. 5I). The overall rates of tumor formation from DU145 cells injected SC and in the yolk of embryonic zebrafish were 35.6% (n = 57/160) for parental cells, 12.8% (n = 22/171) for $\alpha2\beta1^{low}$/$CD44^{low}$ non-adherent (non-TICs) cells, but significantly higher at 58.7% (n = 98/167) for adherent $\alpha2\beta1^{hi}$/$CD44^{hi}$ (TICs) cells ($P < 0.001$; Supplementary Table SI). SC injections yielded an overall higher tumor formation rates than yolk transplants (Supplementary Table SI). Disseminated colonies of QD-labeled cells at >5 distant sites

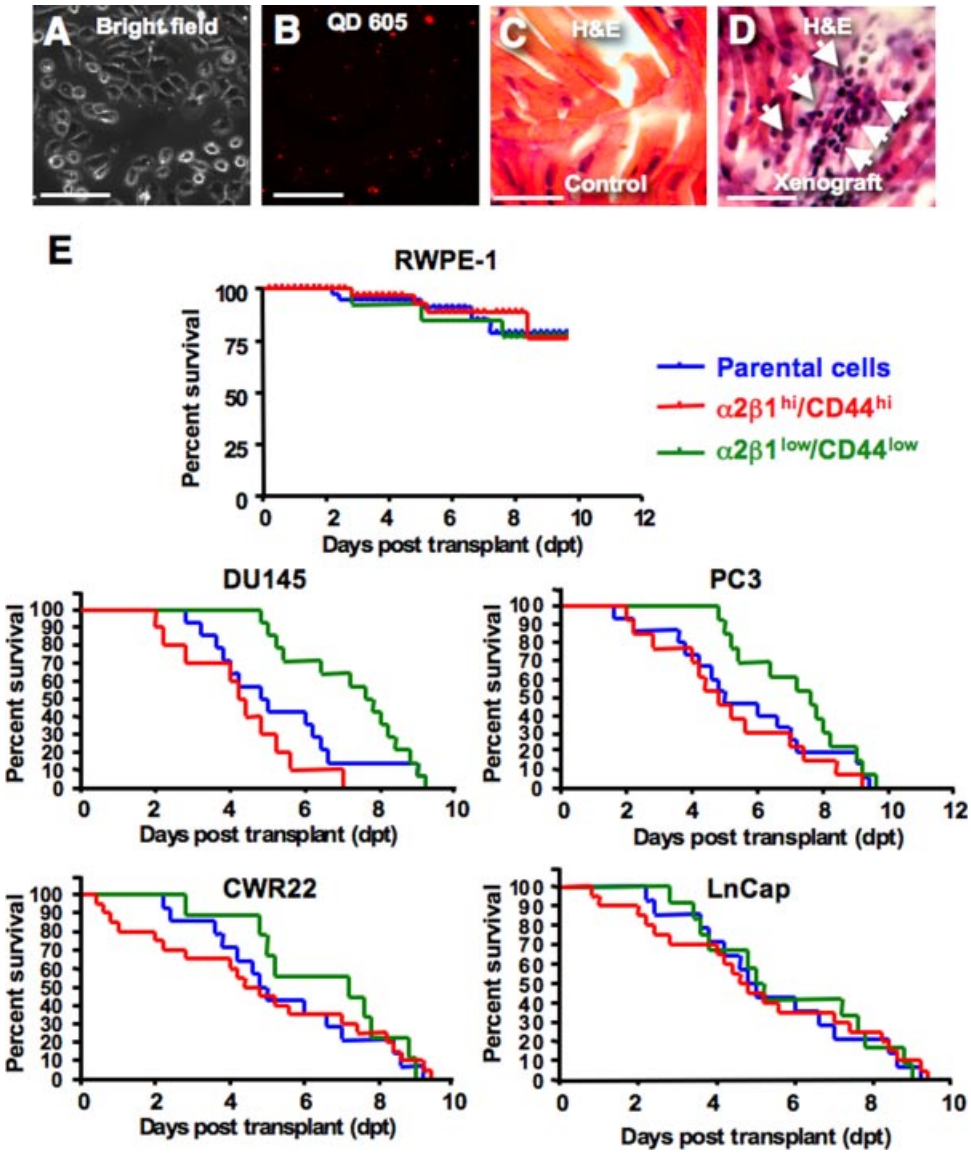

Fig. 4. Zebrafish xenografts of human prostate cancer cells. **A**–**D**: Bright filed image in (A), and the corresponding red (605) fluorescent image in (B) demonstrating efficient labeling of DUI45 cells with quantum dots-605 (QD) in nearly all the cells in the field. C,D: Histological H&E sections from a control non-transplanted zebrafish muscle tissues in (C), compared to a muscle section from DUI45 TICs transplanted fish in (D). Section demonstrates tumor infiltrates with cells resembling morphology of DUI45 cells in fish tissues. Scale bar is 100 μM in (A–D). **E**: Kaplan–Meier survival curve of embryos transplanted with normal prostate cells and multiple PCa cells lines using three fractions; parental (blue), 5′ adherent $\alpha 2\beta 1^{hi}/CD44^{hi}$ cells (TICs; red), and 20 min non-adherent $\alpha 2\beta 1^{low}/CD44^{low}$ (green) cells. Embryos transplanted with cancer cells had significantly shorter survival rates compared to normal prostate cells due to the rapid development of disseminated tumors. The TICs fraction induced significantly higher mortality rates from tumor growth with DUI45, PC3, and CWR22 but not LnCap cells when compared to parental and non-TICs transplants.

were identified at a significantly higher frequencies in xenografts from TICs than from parental or non-TICs. Dissemination rates of SC or into yolk injections were 69%, 39% in 10-parental-cell-, and 26%, 29% in 3-parental-cell-transplants, were 21%, 9% in 10-cell-non-TICs and 17%, 10% for 3-cell-non-TICs transplants, and were 80%, 55% for 10-TIC, and 49%, 52% for 3-TIC-transplants (Supplementary Table SI). Similar results were obtained with PC3, CWR22, LNCap PCa cells. Moreover, PC3 adherent $\alpha 2\beta 1^{low}/CD44^{low}$ cells showed a significantly higher tumor initiation potential than PC3 non-TICs (Supplementary Table SII), suggesting that collagen adhesion might enrich for TICs with added phenotypes to α2β1/CD44 expression.

We next isolated TICs from primary PCa to examine their ability to initiate zebrafish xenografts similar to PCa cell lines. PCa used were diagnosed based on

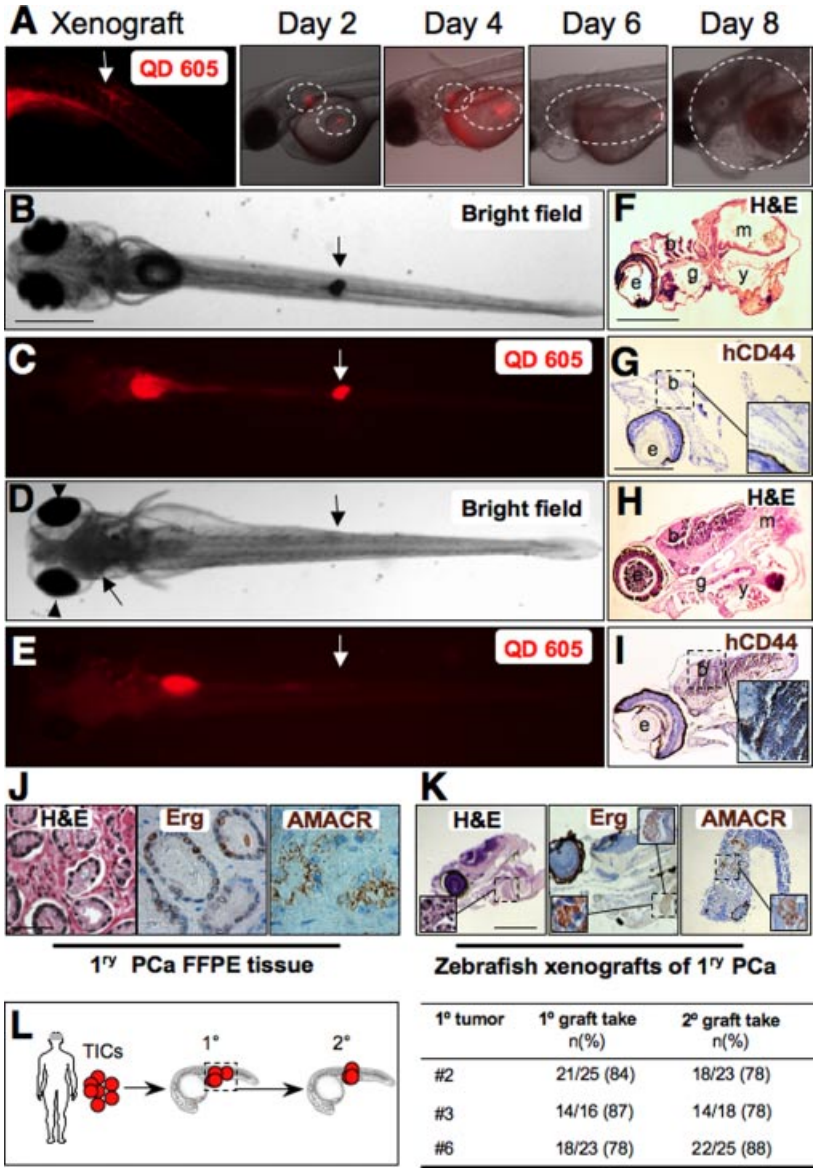

1° tumor	1° graft take n(%)	2° graft take n(%)
#2	21/25 (84)	18/23 (78)
#3	14/16 (87)	14/18 (78)
#6	18/23 (78)	22/25 (88)

Fig. 5. Prostate cancer xenograft tumor progression in zebrafish. **A**: QD 605 red fluorescent image of the site of injection on the left taken on the same day of transplanting primary PCa cells SC in zebrafish embryos. Red and bright image overlays represent sequential imaging of the same xenograft embryo over time during 8 days of tumor growth. From day 2, notice the two sites that are outlined with tumor cells labeled with QD. Tumor growth increases progressively while fluorescence decreases due to QD dilution with cell division. **B**–**E**: Sections from control and PCa xenografts with brain metastasis (D–E). Images were taken at 9 dpt. Downward arrows indicate the site of SC transplantation. Upward arrows in (D and E) on the left indicate cell masses invading the brain and causing exophthalmus (arrowheads in D, compare with no brain metastasis in B). **F**–**K**: H&E staining (F and H) and IHC with anti-human CD44 (G and I) in a representative control untransplanted embryo (F–G) compared to histological sections from a representative xenotransplanted embryo (H–I) with brain metastasis stained with H&E (H) and IHC staining of the same brain region containing disseminated human cells identified with the human isoform-specific anti-CD44 antibody (Inset; H and I). Letters indicate e, eye; b, brain; m, muscle; y, yolk. Insets in panels (G) and (I) are higher magnification of the outlined brain areas, respectively. J: Formalin fixed paraffin embedded (FFPE) sections from a representative primary prostate cancer (PCa) tissue used that are stained with H&E, or in IHC with either Erg or AMACR in brown. The H&E image in (J) is a higher magnification of the outlined areas in Supplementary Figure S4C, while The Erg and AMACR images in (J) are higher magnifications of the outlined areas in Supplementary Figure S6H and F, respectively. K: Sections from zebrafish embryo with PCa xenograft using cells from tissues shown in (K) and stained with H&E, and IHC for Erg and AMACR. Insets are higher magnification of the outlined area in (K). **L**: Diagram demonstrating strategy to study tumor initiation potential of primary PCa cell grafts in secondary xenografts. TICs from the 5 min adherent $\alpha 2\beta 1^{hi}$/$CD44^{hi}$ cells of three patient samples #2, #3, and #6 were transplanted to generate primary xenografts (I). Xenograft tumor areas were dissected, pooled, and TICs were sorted and injected into secondary recipients. Table on the right demonstrates primary and secondary graft take rates. Scale bars are 100 μm in (B–E), (F–J), and (N–K).

histological examination of H&E stained slides (Supplementary Fig. S4). To confirm that zebrafish xenografts were derived from PCa cells and not from benign or normal epithelial cells, we utilized the expression of AMACR and overexpression of Erg as PCa-specific biomarkers [14]. We first optimized the detection of Erg and AMACR by IHC in PCa tissues (Supplementary Fig. S5). We then identified primary PCa cells harboring ERG gene rearrangements determined by interphase FISH (Supplementary Fig. S6), and examined Erg expression in the mirror sections of sampled PCa tissue and after formation of fish xenografts.

Indeed, tumor cells in the mirror section (Fig. 5J, and Supplementary Figs. S5 and S6) and zebrafish xenografts (Fig. 5K) showed strong immunoreactivity with antibodies against AMACR and Erg, suggesting that these zebrafish xenografts are derived from PCa cells. Further analysis of human PCa cells in xenografts derived from adherent $\alpha2\beta1^{hi}/CD44^{hi}$ (TICs) that frequently disseminated to the brain region of zebrafish embryos (Fig. 5H–I), or migrated to the tail (Supplementary Fig. S7A–D) demonstrated that many (but not all) of these cells were positive for CD44 expression (evidence for formation of $CD44^{-}$ cells, or CD44 plasticity), and demonstrated features of potential cell differentiation including the expression of CK8/18 (Supplementary Fig. S7C and D), a clinical marker used to identify luminal and/or intermediate PCa cells. Furthermore, IHC analyses of xenografts from primary PCa cells demonstrated that cells in these xenografts coexpress the prostate-specific marker PSA and the human-specific CD44 isoform (Supplementary Fig. S7E–H).

Importantly, to examine if TICs derived from zebrafish xenografts of primary PCa retain their abilities for serial tumor transplantation, we sorted labeled tumor cells from primary fish xenografts, and used them for secondary xenografts (Fig. 5L). TICs from primary grafts were able to initiate secondary xenografts in 81.8% of cases ($n = 54/66$ secondary xenograft embryo from three patient samples). Thus, PCa xenografts in zebrafish are derived from TICs that can retain genotypic and phenotypic features, some differentiation potential, and serial tumor transplantation ability of human PCa cells, and similar to mouse xenografts, the $\alpha2\beta1^{hi}/CD44^{hi}$ cells are more tumorigenic in zebrafish embryos.

Assessing the Frequencies of Prostate Tumor-Initiating Cells Using Zebrafish Xenografts

TIC frequency of human PCa cells in zebrafish xenografts were determined using ELDA [29] (Supplementary Fig. S8) from SC transplantation of parental, 5 min adherent $\alpha2\beta1^{hi}/CD44^{hi}$ cells, and 20 min non-adherent $\alpha2\beta1^{low}/CD44^{low}$ cells in limiting dilutions. Self-renewing TICs were found to be abundant, and comprised 0.3–1.3% of DU145 cells (Supplementary Fig. S8) and 0.02–0.9% of PC3 cells.

We also isolated the 5 min adherent $\alpha2\beta1^{hi}/CD44^{hi}$ cells (TICs) from six primary PCa patients (Table I) from prostatectomies, and examined their tumor initiation potential in zebrafish xenografts. TICs from primary PCa tissues engrafted robustly in the pre-immune zebrafish embryos at rates higher than that of PCa cell lines (Supplementary Table SIII). Self-renewing TICs from primary tumors varied from scarce to widely abundant compared to PCa cell lines, and comprised 0.22% (1/456) to 14.3% (1/7) of primary PCa cells (Table I).

To study whether the tumorigenic ability of prostate TICs in zebrafish is restricted to transplants in the immune-tolerant embryonic microenvironment, we used prednisone-conditioned juvenile transparent Casper [18] zebrafish as recipients. DU145 parental cells, 5 min adherent $\alpha2\beta1^{hi}/CD44^{hi}$ cells, and 20 min non-adherent $\alpha2\beta1^{low}/CD44^{low}$ cells were transplanted, and fish were monitored at 33°C. Prostate TICs injected SC initiated visible tumors in juvenile fish after an average of 13 days (Supplementary Fig. S9), and then invaded both local and remote tissues by day 28 (Supplementary Fig. S9C). Histological analyses of tumor masses demonstrate cells with engrafted DU145 morphology (Inset in Supplementary Fig. S9B). Whether injected SC in the tail region (Supplementary Fig. S9B and C), or IP (Supplementary Fig. S9D and E), tumors from parental and TIC DU145 cells disseminated to distal sites (Supplementary Table SIV). The overall rates of tumor dissemination of 10-500 DU145 cells injected SC and IP in conditioned juvenile fish were 77.8% ($n = 14/18$) with parental cells, 22.2% ($n = 4/18$) with Non-TICs, and 88.8% ($n = 16/18$) with TICs (Supplementary Table SIV). Importantly, benign prostate epithelial cells survived but failed to initiate tumors in zebrafish (Supplementary Table SI). Collectively, these data suggest that 5 min adherent $\alpha2\beta1^{hi}/CD44^{hi}$ TICs derived from PCa cell lines and primary PCa cells are more tumorigenic in zebrafish xenografts.

DISCUSSION

The presence of distinct subpopulations of TICs in solid tumors has proved contentious [35,36]. However, the evidence for a central role of TICs in tumor growth has most recently been solidified by lineage tracing studies in mice [5–7]. We examined the expression of stem cell markers in multiple PCa cell lines, and found PCa TICs to have increased expression of $\alpha2\beta1$-

integrin and CD44. We confirmed that TICs derived from primary PCa tissues shared identical properties. We performed several functional assays including colony and serial spheroid formation, migration, and invasion assays, and tumor xenograft studies. We demonstrate that $\alpha2\beta1^{hi}/CD44^{hi}$ cells robustly adhere to collagen, elevate CD133 reflecting increased abilities to initiate serially passageable spheres when grown as spheroids, are able to self-renew as single cells in serial spheroid assays, and have enhanced tumor initiation abilities in mice and zebrafish. We identified the rapidly adherent $\alpha2\beta1^{hi}/CD44^{hi}$ subfraction to consistently contain prostate TICs independent of CD133 expression among all PCa cells that we have examined. Previous studies provided strong evidence for CD133 as a prostate TIC marker [37,38]. Similarly, we have shown here that CD133 expression is elevated in prostate spheres. However, other studies in PCa and other cancers showed tumor initiation independent of CD133 expression [39–42]. The apparent inconsistency of CD133 expression in prostate TICs likely reflects tumor heterogeneity, marker plasticity in response to changes in the niche during PCa clonal evolution, its minute levels (~0.01%), and the necessity for correct CD133 glycosylation and protein folding for precise marking of stem cells [43].

Tumor cells that possess substantial replicative ability might be stem cell-like cells with self-renewing abilities, or mutated transit-amplifying cells without self-renewal capacity [44–46], and the self-renewal states might evolve during the clonal selection process [46]. Multiple molecular pathways regulate the biology of stem cells and self-renewal features, and are therefore potential targets in TICs [47]. Among these reticulate pathways are Bmi-1, Oct3/4, Hedgehog (Hh), Wnt/β-catenin, Notch signaling, Hox gene family, PTEN/Akt pathway, efflux transporters such as ABCG markers of self-renewal, and upregulated telomerase activity [48]. Studies suggest that Bmi-1 is necessary for Hh- [49], and β-catenin-mediated self-renewal [50] making Bmi-1 one of the most critical self-renewal targets. Thus, the zebrafish xenograft model of tumor initiation that we developed might help to identify inhibitors targeting these critical self-renewal pathways.

Self-renewal is likely a dynamic feature by which cancer cells respond to changes in the microenvironment. Accordingly, the relative frequency of TICs is likely to vary between experimental systems utilizing distinct readouts, microenvironments, and tumor types. We have utilized ELDA, rather than LDA to determine TIC frequencies, since ELDA have the capacity to calculate frequencies for stem cell subpopulations that produce 0% or 100% tumor engraftment [29]. Importantly, we have used zebrafish embryos to develop rapid xenografts of primary PCa cells (within 12 days), and to determine that the frequencies of self-renewing primary PCa cells are more abundant in the immune-permissive zebrafish embryonic microenvironment. Our data provide further evidence for an inverse relationship between the TIC frequency and immune competency of the xenograft recipient [51], and highlight the importance of developing better xenograft models.

Since primary PCa cells are difficult to propagate in mouse xenografts, an approach that is recently adapted in order to increase survival of primary prostate xenografts is tissue recombination of primary PCa cells with inductive stroma [52] by utilizing neonatal mouse mesenchyme [53]. It is increasingly critical to determine if coculture with embryonic heterologous stromal component that promotes epithelial proliferation and differentiation alters the TIC properties of adult prostate epithelial progenitors [54]. Human PCa cells retained many of their phenotypic, differentiation, and serial transplantation features, and displayed metastatic dissemination behavior in zebrafish. Thus, zebrafish xenografts recapitulate a broad spectrum of engrafted PCa cell biology and dissemination behavior, and may be developed to screen for small-molecule inhibitors that target self-renewal to control progression and recurrence of multiple cancers.

ACKNOWLEDGMENTS

We thank Dr. Leonard Zon (Harvard) for Casper zebrafish, and Kathleen Flaherty for technical assistance and fish maintenance. This study was supported in part by the NCI CCSG award (P30CA072720), and received funding from Department of Defense Prostate Cancer Grants (W81XWH-12-1-0251 to H.S., J.B., I.K.), and Rutgers Cancer Institute of New Jersey (Pilot Grant to J.B., H.S.).

REFERENCES

1. Isaacs JT. Control of cell proliferation and cell death in the normal and neoplastic prostate: A stem cell model. In: Rodgers CHCD, Cunha G, Grayhack JT, Hinman F Jr, Horton R, editors. Benign prostatic hyperplasia. Washington, DC: US Department of Health and Human Services; 1987. pp. 85–94.
2. Isaacs JT, Kyprianou N. Biological basis for chemohormonal therapy for prostatic cancer. Cancer Treat Res 1989;46:177–193.
3. Collins AT, Berry PA, Hyde C, Stower MJ, Maitland NJ. Prospective identification of tumorigenic prostate cancer stem cells. Cancer Res 2005;65(23):10946–10951.
4. Dick JE. Stem cell concepts renew cancer research. Blood 2008;112(13):4793–4807.
5. Chen J, Li Y, Yu TS, McKay RM, Burns DK, Kernie SG, Parada LF. A restricted cell population propagates glioblastoma growth after chemotherapy. Nature 2012;488(7412):522–526.

6. Driessens G, Beck B, Caauwe A, Simons BD, Blanpain C. Defining the mode of tumour growth by clonal analysis. Nature 2012;488(7412):527–530.
7. Schepers AG, Snippert HJ, Stange DE, van den Born M, van Es JH, van de Wetering M, Clevers H. Lineage tracing reveals lgr5+ stem cell activity in mouse intestinal adenomas. Science 2012;337 (6095):730–735.
8. Ishii H, Iwatsuki M, Ieta K, Ohta D, Haraguchi N, Mimori K, Mori M. Cancer stem cells and chemoradiation resistance. Cancer Sci 2008;99(10):1871–1877.
9. Danila DC, Heller G, Gignac GA, Gonzalez-Espinoza R, Anand A, Tanaka E, Lilja H, Schwartz L, Larson S, Fleisher M, Scher HI. Circulating tumor cell number and prognosis in progressive castration-resistant prostate cancer. Clin Cancer Res 2007;13 (23):7053–7058.
10. Patrawala L, Calhoun-Davis T, Schneider-Broussard R, Tang DG. Hierarchical organization of prostate cancer cells in xenograft tumors: The cd44+ alpha2beta1+ cell population is enriched in tumor-initiating cells. Cancer Res 2007;67(14):6796–6805.
11. Berezovska OP, Glinskii AB, Yang Z, Li XM, Hoffman RM, Glinsky GV. Essential role for activation of the polycomb group (pcg) protein chromatin silencing pathway in metastatic prostate cancer. Cell Cycle 2006;5(16):1886–1901.
12. Choi N, Zhang B, Zhang L, Ittmann M, Xin L. Adult murine prostate basal and luminal cells are self-sustained lineages that can both serve as targets for prostate cancer initiation. Cancer Cell 2012;21(2):253–265.
13. Tomlins SA, Rhodes DR, Perner S, Dhanasekaran SM, Mehra R, Sun XW, Varambally S, Cao X, Tchinda J, Kuefer R, Lee C, Montie JE, Shah RB, Pienta KJ, Rubin MA, Chinnaiyan AM. Recurrent fusion of tmprss2 and ets transcription factor genes in prostate cancer. Science 2005;310(5748):644–648.
14. Chaux A, Albadine R, Toubaji A, Hicks J, Meeker A, Platz EA, De Marzo AM, Netto GJ. Immunohistochemistry for erg expression as a surrogate for tmprss2-erg fusion detection in prostatic adenocarcinomas. Am J Surg Pathol 2011;35(7):1014–1020.
15. Jones PH, Harper S, Watt FM. Stem cell patterning and fate in human epidermis. Cell 1995;80(1):83–93.
16. Collins AT, Habib FK, Maitland NJ, Neal DE. Identification and isolation of human prostate epithelial stem cells based on alpha (2)beta(1)-integrin expression. J Cell Sci 2001;114(Pt 21):3865–3872.
17. Zon LI, Peterson RT. In vivo drug discovery in the zebrafish. Nat Rev Drug Discov 2005;4(1):35–44.
18. White RM, Sessa A, Burke C, Bowman T, LeBlanc J, Ceol C, Bourque C, Dovey M, Goessling W, Burns CE, Zon LI. Transparent adult zebrafish as a tool for in vivo transplantation analysis. Cell Stem Cell 2008;2(2):183–189.
19. Stoletov K, Montel V, Lester RD, Gonias SL, Klemke R. High-resolution imaging of the dynamic tumor cell vascular interface in transparent zebrafish. Proc Natl Acad Sci USA 2007;104 (44):17406–17411.
20. Nicoli S, Ribatti D, Cotelli F, Presta M. Mammalian tumor xenografts induce neovascularization in zebrafish embryos. Cancer Res 2007;67(7):2927–2931.
21. Marques IJ, Weiss FU, Vlecken DH, Nitsche C, Bakkers J, Lagendijk AK, Partecke LI, Heidecke CD, Lerch MM, Bagowski CP. Metastatic behaviour of primary human tumours in a zebrafish xenotransplantation model. BMC Cancer 2009;9:128.
22. Quintana E, Shackleton M, Sabel MS, Fullen DR, Johnson TM, Morrison SJ. Efficient tumour formation by single human melanoma cells. Nature 2008;456(7222):593–598.
23. Patrawala L, Calhoun T, Schneider-Broussard R, Zhou J, Claypool K, Tang DG. Side population is enriched in tumorigenic, stem-like cancer cells, whereas abcg2+ and abcg2− cancer cells are similarly tumorigenic. Cancer Res 2005;65(14):6207–6219.
24. Xin L, Lawson DA, Witte ON. The sca-1 cell surface marker enriches for a prostate-regenerating cell subpopulation that can initiate prostate tumorigenesis. Proc Natl Acad Sci USA 2005;102 (19):6942–6947.
25. Croker AK, Goodale D, Chu J, Postenka C, Hedley BD, Hess DA, Allan AL. High aldehyde dehydrogenase and expression of cancer stem cell markers selects for breast cancer cells with enhanced malignant and metastatic ability. J Cell Mol Med 2009;13(8B):2236–2252.
26. Tomayko MM, Reynolds CP. Determination of subcutaneous tumor size in athymic (nude) mice. Cancer Chemother Pharmacol 1989;24(3):148–154.
27. Kramer J, Granier CJ, Davis S, Piso K, Hand J, Rabson AB, Sabaawy HE. Pdcd2 controls hematopoietic stem cell differentiation during development. Stem Cells Dev 2013;22(1):58–72.
28. Sabaawy HE, Azuma M, Embree LJ, Tsai HJ, Starost MF, Hickstein DD. Tel-aml1 transgenic zebrafish model of precursor b cell acute lymphoblastic leukemia. Proc Natl Acad Sci USA 2006;103(41):15166–15171.
29. Hu Y, Smyth GK. Elda: Extreme limiting dilution analysis for comparing depleted and enriched populations in stem cell and other assays. J Immunol Methods 2009;347(1–2):70–78.
30. Hurt EM, Kawasaki BT, Klarmann GJ, Thomas SB, Farrar WL. Cd44+ cd24(−) prostate cells are early cancer progenitor/stem cells that provide a model for patients with poor prognosis. Br J Cancer 2008;98(4):756–765.
31. Goldstein AS, Lawson DA, Cheng D, Sun W, Garraway IP, Witte ON. Trop2 identifies a subpopulation of murine and human prostate basal cells with stem cell characteristics. Proc Natl Acad Sci USA 2008;105(52):20882–20887.
32. Li A, Simmons PJ, Kaur P. Identification and isolation of candidate human keratinocyte stem cells based on cell surface phenotype. Proc Natl Acad Sci USA 1998;95(7):3902–3907.
33. Shinohara T, Orwig KE, Avarbock MR, Brinster RL. Spermatogonial stem cell enrichment by multiparameter selection of mouse testis cells. Proc Natl Acad Sci USA 2000;97(15):8346–8351.
34. Vazquez-Martin A, Oliveras-Ferraros C, Del Barco S, Martin-Castillo B, Menendez JA. The anti-diabetic drug metformin suppresses self-renewal and proliferation of trastuzumab-resistant tumor-initiating breast cancer stem cells. Breast Cancer Res Treat 2010;126(2):355–364.
35. Visvader JE, Lindeman GJ. Cancer stem cells in solid tumours: Accumulating evidence and unresolved questions. Nat Rev Cancer 2008;8(10):755–768.
36. Rosen JM, Jordan CT. The increasing complexity of the cancer stem cell paradigm. Science 2009;324(5935):1670–1673.
37. Vander Griend DJ, Karthaus WL, Dalrymple S, Meeker A, DeMarzo AM, Isaacs JT. The role of cd133 in normal human prostate stem cells and malignant cancer-initiating cells. Cancer Res 2008;68(23):9703–9711.
38. Richardson GD, Robson CN, Lang SH, Neal DE, Maitland NJ, Collins AT. Cd133, a novel marker for human prostatic epithelial stem cells. J Cell Sci 2004;117(Pt 16):3539–3545.

39. Taylor RA, Toivanen R, Frydenberg M, Pedersen J, Harewood L, Australian Prostate Cancer B, Collins AT, Maitland NJ, Risbridger GP. Human epithelial basal cells are cells of origin of prostate cancer, independent of cd133 status. Stem Cells 2012;30 (6):1087–1096.
40. Zhou J, Wang H, Cannon V, Wolcott KM, Song H, Yates C. Side population rather than cd133(+) cells distinguishes enriched tumorigenicity in htert-immortalized primary prostate cancer cells. Mol Cancer 2011;10:112.
41. Pfeiffer MJ, Schalken JA. Stem cell characteristics in prostate cancer cell lines. Eur Urol 2009;57(2):246–254.
42. Pellacani D, Packer RJ, Frame FM, Oldridge EE, Berry PA, Labarthe MC, Stower MJ, Simms MS, Collins AT, Maitland NJ. Regulation of the stem cell marker cd133 is independent of promoter hypermethylation in human epithelial differentiation and cancer. Mol Cancer 2011;10:94.
43. Pellacani D, Oldridge EE, Collins AT, Maitland NJ. Prominin-1 (cd133) expression in the prostate and prostate cancer: A marker for quiescent stem cells. Adv Exp Med Biol 2013;777:167–184.
44. Hemmati HD, Nakano I, Lazareff JA, Masterman-Smith M, Geschwind DH, Bronner-Fraser M, Kornblum HI. Cancerous stem cells can arise from pediatric brain tumors. Proc Natl Acad Sci USA 2003;100(25):15178–15183.
45. Singh SK, Clarke ID, Terasaki M, Bonn VE, Hawkins C, Squire J, Dirks PB. Identification of a cancer stem cell in human brain tumors. Cancer Res 2003;63(18):5821–5828.
46. Nowell PC. The clonal evolution of tumor cell populations. Science 1976;194(4260):23–28.
47. Mimeault M, Batra SK. Frequent gene products and molecular pathways altered in prostate cancer- and metastasis-initiating cells and their progenies and novel promising multitargeted therapies. Mol Med 2011;17(9–10):949–964.
48. Reya T, Morrison SJ, Clarke MF, Weissman IL. Stem cells, cancer, and cancer stem cells. Nature 2001;414(6859):105–111.
49. Liu S, Dontu G, Mantle ID, Patel S, Ahn NS, Jackson KW, Suri P, Wicha MS. Hedgehog signaling and bmi-1 regulate self-renewal of normal and malignant human mammary stem cells. Cancer Res 2006;66(12):6063–6071.
50. Bisson I, Prowse DM. Wnt signaling regulates self-renewal and differentiation of prostate cancer cells with stem cell characteristics. Cell Res 2009;19(6):683–697.
51. O'Brien CA, Kreso A, Jamieson CH. Cancer stem cells and self-renewal. Clin Cancer Res 2010;16(12):3113–3120.
52. Goldstein AS, Drake JM, Burnes DL, Finley DS, Zhang H, Reiter RE, Huang J, Witte ON. Purification and direct transformation of epithelial progenitor cells from primary human prostate. Nat Protoc 2011;6(5):656–667.
53. Toivanen R, Berman DM, Wang H, Pedersen J, Frydenberg M, Meeker AK, Ellem SJ, Risbridger GP, Taylor RA. Brief report: A bioassay to identify primary human prostate cancer repopulating cells. Stem Cells 2011;29(8):1310–1314.
54. Risbridger GP, Taylor RA. Minireview: Regulation of prostatic stem cells by stromal niche in health and disease. Endocrinology 2008;149(9):4303–4306.

SUPPORTING INFORMATION

Additional supporting information may be found in the online version of this article at the publisher's web-site.

SUPPLEMENTARY DATA

Enrichment of human prostate cancer cells with tumor initiating properties in mouse and zebrafish xenografts by differential adhesion

Nitu Bansal, Stephani Davis, Irina Tereshchenko, Tulin Budak-Alpdogan, Hua Zhong, Mark N. Stein, Isaac Yi Kim, Robert S. DiPaola, Joseph R. Bertino, Hatem E. Sabaawy

SUPPLEMENTARY METHODS

Cell Culture, prostate spheres, colony formation, migration, and invasion assays

Prostate cancer cells Du145, PC3, CWR22 and LnCap cells were generated from stocks maintained at CINJ, and were originally purchased from ATCC. Cells were cultured at low passage numbers in RPMI media (GIBCO) supplemented with 10% fetal bovine serum (FBS), and 1% penicillin-streptomycin. For all the attachment experiments, early passage cells were used. For colony forming and clonogenic assays, 200 prostate cancer cells were plated in 6-well plates. After 2 weeks, the plates were washed in 1x PBS, and cells were stained with crystal violet. Colonies of >50 cells were counted. Prostate spheres were generated in 1% agarose in keratinocyte serum free media (KSFM) media. The spheroids grown on 1% agarose were cultured in KSFM supplemented with epidermal growth factor (EGF), basic fibroblast growth factor (bFGF), and bovine pituitary extract (All from Invitrogen) (1). Collagen-I-adherent cells at 5 minutes, and non-adherent cells after 20 minutes were suspended at 2 x 10^3 cells/well in KSFM media. Every 3 days, half of the media was replaced, and spheres consisting of >50 cells were counted on day14. Single cells from day-7 spheroids were used in secondary spheroid assays. RWPE (normal prostate cells) were also cultured in KSFM as recommended by ATCC.

In migration assays, cells were plated in 0.5% FBS media in transwell chambers with the lower chambers contained growth media with 10% FBS. After 48 hrs, cells that migrated to the lower surface of transwell inserts were stained with crystal violet and counted. In invasion assays, cells were plated on matrigel-coated transwell inserts and assayed.

Primary prostate cancer tissue dissociation and culture of primary cells

Human primary prostate cancer tissues were obtained by radical prostatectomy (IRB approved). For isolation of single cells, the tissue was minced into smaller pieces and incubated for 2-4 hrs at 37ºC in RPMI media supplemented with 10% FBS, 1% Anti-anti (Invitrogen), 200U/ml collagenase I (Sigma Aldrich, USA), 0.5mg/ml Dispase II (Stem Cell

Technologies). After 4 hrs, the digested tissue pieces were filtered through 100 μm cell strainers (BD Falcon), and centrifuged at 250g for 30 seconds. Cell pellets were then washed once with 1xPBS and centrifuged once more at 250g for 30 seconds. The final cell pellet was suspended in prosta life media (Lifeline Technologies) and plated in T25 flasks. The media was changed once every 3 days.

Flow cytometry and cytotoxicity assays

Cells obtained after attachment assay or after treatments were collected and washed twice in 1xPBS. 1x 10^6 cells were then suspended in 1xPBS and stained with the antibodies conjugated with either FITC or PE and APC. After 30 mins of incubation in dark, cells were washed with PBS and suspended in 5μl of 7AAD. The cells were then acquired using FACS Calibur instrument. Both acquisition and analysis were done using Cell Quest software. Antibodies used for flow were CD49b (β1-Integrin)-FITC (Millipore), CD44-APC, CD133-PE and 7-AAD (purchased from DB Biosciences). Cytotoxicity of methotrexate and other chemotherapies were assayed following a 3-day exposure. Prostate cancer cells (3 x 10^3 cells/well) were treated with multiple concentrations to determine an IC_{50}, cell growth was monitored over time and resulting cytotoxicity was analyzed using MTS assay (Sigma) per manufacturer's instructions.

IHC for validation of prostate cancer epithelium and chromosomal rearrangements

Each prostate cancer sample was subjected at diagnosis to histological examination of the H&E slides to determine tumor regions, and consecutively cut slides from these core regions were utilized for IHC and interphase FISH. For IHC, formalin fixed paraffin-embedded (FFPE) tissue samples from biopsies and xenografts were stained with selected antibodies using antigen retrieval, and sections were scored for percentage of cells and intensity on a 0-2 scale by pathologists blinded to cell fractions. First, the H&E slide and α-methylacyl-coenzyme-A racemase (AMACR)-immunostained sections were reviewed by qualified pathologists. Overexpression of AMACR in prostate cancer cells was detected by IHC using a monoclonal rabbit anti-human P504S antibody (clone 13H4, Cell Marque). After tumor regions were determined, consecutive slides were included in FISH analysis. Overexpression of ERG gene in prostate cancer cells that were harboring TMPRSS2-Erg fusion was detected by IHC using a monoclonal rabbit anti-human ERG antibody (clone EP111, Dako).

Interphase FISH validation of rearrangements

ERG gene rearrangement was assessed using a newly developed break-apart interphase FISH assay optimized from a previously described protocol (2) with modifications. In brief, the TMPRSS2-Erg rearrangement probes were optimized to detect the deletion between TMPRSS2 and ERG at 21q22 associated with the TMPRSS2-Erg fusion in a triple-color deletion assay. Optimization included the incorporation of additional bacterial artificial chromosome (BAC) probes for the detection of gene fusions (Irina Tereshchenko and Robert S. DiPaola; unpublished data). All BACs were obtained from the BACPAC Resource Center (Oakland, CA, USA). DNA probes were synthesized using 5-(3-aminoallyl)-dUTP-nick translation and the ARES Alexa Fluor DNA Labeling Kit (Molecular Probes, Invitrogen, USA). For detection of ERG rearrangements and TMPRSS2-ERG fusion, we used the following probes: RP11-95I21 (Alexa Fluor 555-labeled; 5' to ERG), RP11-476D17 (Alexa Fluor 488-labeled; 3' to ERG), and RP11-35C4 (Alexa Fluor 647-labeled; 5' to TMPRSS2). Labeled samples on FISH slides were scanned using a confocal microscope (Zeiss LSM 510 META, 100x objective). Image stacks of 300 nm z-step size were captured and analyzed using Imaris Software (Bitplane). At least 50-100 nuclei were evaluated per tissue section, whenever it was possible.

Extreme Limiting dilution analysis (ELDA)

To assess the number of self-renewing cells contained within the bulk of the primary prostate cancer mass, QD-labeled primary prostate cancer cells were propagated and 5 min collagen-attached $\alpha2\beta1^{hi}$/$CD44^{hi}$ cells were isolated, and introduced SC into 48 hpf zebrafish recipients at limiting dilution (1×10^3, 1×10^2, 1×10^1, and 3 cells/embryo), with purity of 98-99%, and viability 95-99.9% (n=50 embryos injected/tumor case). Engraftment was assessed starting at 5 days post transplantation by fluorescence microscopy. Embryos that showed engraftment at day 5 and latter on died from disseminated tumors were scored positive for tumor initiation. The TIC frequency was finally calculated after 12 dpt using linear regression method completed using ELDA at http://bioinf.wehi.edu.au/cgi-bin/limdil/limdil.pl. ELDA have the capacity to calculate frequencies for stem cell subpopulations that produce 0% or 100% tumor engraftment, and therefore is preferred for calculating tumor initiation from limited cell numbers. Accuracy of this test is determined by correlation coefficient (R^2 values), and provided 99% confidence intervals to compare tumor-initiating cell numbers between samples. To verify these data, we have also used L-Calc statistical software (Stem cell technologies) for limiting dilution analysis

(LDA), and subsequent analyses provided 95% confidence intervals and *t* test statistical values that distinguished between the numbers of TIC from the three fractions of cells investigated.

SUPPLEMENTARY REFERENCES

1. Mimeault M, Johansson SL, Batra SK. Pathobiological implications of the expression of EGFR, pAkt, NF-kappaB and MIC-1 in prostate cancer stem cells and their progenies. PLoS One 2012;7:e31919.

2. Mehra R, Tomlins SA, Shen R, et al. Comprehensive assessment of TMPRSS2 and ETS family gene aberrations in clinically localized prostate cancer. Mod Pathol 2007;20:538-44.

SUPPLEMENTARY FIGURE LEGEND

Supplementary Fig 1. Morphology and proliferation of different collagen adherent fractions. **A**: Cell proliferation of the subfractions of collagen adherent cells during culture for 6 days. **B:** Light phase microscopic images of DU145 and PC3 cells after 1 and 6 days of culture. Images are taken at 10X magnification. DU145 cells were most confluent at imaging. Scale bar is 100 μM in all DU145 and PC3 image panels.

Supplementary Fig. 2. Collagen-adherent cells are enriched in putative TICs. **A:** Mean percentage of 5` adherent and 20` non-adherent fractions of cells with $\alpha2\beta1^{hi}/CD44^{hi}$ phenotype in PC3, PC3 spheroids, CWR22, and CWR22 spheroids. Data represent three independent experiments performed in triplicates. **B:** Flow cytometric analyses of CWR22 and LnCap cells after collagen adherence showing higher mean fluorescence intensity (MFI) of 5 minutes collagen-I-adherent ($\alpha2\beta1^{hi}/CD44^{hi}$) cells (Adherent) compared to 20 min-non-adherent ($\alpha2\beta1^{low}/CD44^{low}$) cells (Non-adherent), and IgG control (IgG). **C:** CD133 expression in various subsets of CWR22 cells. In a representative experiment, 0.1% of the cells were $\alpha2\beta1^{hi}/CD44^{hi}$/CD133 positive, and spheroids from these $\alpha2\beta1^{hi}/CD44^{hi}$ cells showed upregulated CD133 expression to 1.42% (*$p<0.001$).

Supplementary Fig. 3. Self-renewal and *in vitro* tumorigenic potential of collagen-adherent $\alpha2\beta1^{hi}/CD44^{hi}$ cells. **A:** Bars demonstrate the enhanced ability of single $\alpha2\beta1^{hi}/CD44^{hi}$ cells to form spheroids, compared to the limited ability of single $\alpha2\beta1^{low}/CD44^{low}$ cells. **B:** Images from $\alpha2\beta1^{low}/CD44^{low}$-derived spheroids that stopped growing at day 9. Scale bars are 50 μm. **C:** Quantitation of secondary spheroids from $\alpha2\beta1^{hi}/CD44^{hi}$ and $\alpha2\beta1^{low}/CD44^{low}$ single cells derived from primary spheroids at day-7. Numbers of spheroids are displayed as mean ± s.e.m, and were done in triplicate. **D:** IC_{50} concentrations of various drugs used. IC_{50}s were determined using MTS assays in DU145 cells. **E:** DU145 cells were treated with the clinically used chemotherapy drugs at IC_{50} concentrations. Collagen-adherent cells at 5-minutes were measured using MTS assays. Values are represented as mean fold of 5 minute-adhesion ± S.D. from three independent experiments. There was a lack of significant inhibition of 5 min-adhesion in cells treated with taxotere and cisplatinum (# $p>0.05$), a non-significant increase in adhesion with doxorubicin (^ $p>0.05$), and a statistically significant increase in adhesion with methotrexate and carboplatinum (* $p<0.05$) suggesting resistance.

Supplementary Fig 4. Diagnostic images of prostate cancers based on histological H&E examination. **A-F:** Formalin fixed paraffin embedded (FFPE) sections from two representative primary prostate cancer (PCa) tissues used for generating zebrafish xenografts. Sections of PCa tissues from patient #5 (**A-C**) and patient #6 (**D-F**) were stained with H&E, and imaged. The H&E images in **B-C** and **E-F** are higher magnifications of the outlined areas in **A** and **D**, respectively. Inset in **F** is a 500X magnification of the outlined area in the same panel. An H&E image in the main figures (Fig. 5J) represents a 500X magnification of the outlined area (*) in this supplementary Fig.4C from same patient's tissue.

Supplementary Fig 5. Expression of Erg and AMACR in primary PCa tissues. FFPE sections from primary PCa tissues were used to detect the overexpression of both Erg, due to the presence of TMPRESS2:Erg fusions, and AMACR proteins in PCa cells by IHC. **A-D:** Two representative cases of PCa cells that are either negative (**A-B**) or positive (**C-D**) for Erg expression in brown. Notice that in both cases, endothelial cells demonstrated a strongly positive Erg expression (arrow), and were used as an internal positive control. The images in **B** and **D** are higher magnifications of the outlined areas in **A** and **C**, respectively. **E-H:** Two representative cases of PCa cells that are positive for AMACR expression. The sections in (**G-H**) are from the same tissues that are positive for Erg expression in (**C-D**), therefore, Erg overexpression correlates with AMACR expression in these PCa cells that harbor the TMPRESS-Erg fusion. AMARC expression either in brown (**E-F**) or in red (**G-H**) was detected as a strong cytoplasmic granular staining. The images in **F** and **H** are higher magnifications of the outlined areas in **E** and **G**, respectively. An AMACR IHC image in the main figures (Fig. 5J) represents a higher magnification of the outlined area (*) in this supplementary Fig.5F from the same patient's tissue. **I-J:** Dual IHC for Erg and AMACR expression in a section from a PCa patient with no known TMPRSS:Erg fusions. The sections in (**I-J**) are from the same tissues that are negative for Erg expression in (**A-B**), therefore, AMACR expression may be used to identify PCa cells that do not express Erg when these PCa cells do not harbor the TMPRESS-Erg fusion. Notice that endothelial cells demonstrated a strongly positive Erg expression (arrow), and were used as an internal positive control.

Supplementary Fig 6. Expression of Erg and AMACR in primary PCa cells harboring the TMPRESS-Erg fusion and were used to generate zebrafish xenografts of primary PCa cells. **A-F:** Control sections from primary PCa tissues known to overexpress Erg, due to the presence of TMPRESS2:Erg fusion. **A:** H&E. **B:** Erg overexpression. **C:** AMACR overexpression. **D-E:** Dual Erg/AMACR expression in PCa cells by IHC. The image in **E** is a higher magnification of the

outlined area in **D**. **F:** Multicolor interphase FISH on cells from the same patient tissues in A-E demonstrating TMPRESS:Erg rearrangements. The translocation is demonstrated through split of red and green signals representing the rearranged ERG allele, while juxtaposition of green and white signals (arrow) designates the TMPRESS:Erg fusion. **G-I:** IHC and interphase FISH sections from primary PCa patient #5, with TICs that were used to generate zebrafish xenografts. The image in **H** is a higher magnification of the outlined areas in **G**. An Erg overexpression IHC image in the main figures (Fig. 5J) represents a 500X magnification of the outlined area (*) in this supplementary Fig.6H from a sequential section of the same #5 patient's tissue. **I:** Multicolor interphase FISH on cells from the same #5 patient's tissues in **G-H** demonstrating TMPRESS:Erg rearrangements. The intact ERG allele is designated by juxtaposition of red and green signals. The TMPRESS:ERG gene fusion was detected through deletion with the absence of a red signal and remaining green signal. Please note that TICs from this same primary PCa patient #5 were used to generate zebrafish xenografts, and cells from these xenografts showed strong nuclear staining for Erg by IHC (Fig. 5J), suggesting that these fish xenografts were derived from primary PCa cells, and not from normal epithelial cells. Scale bars are 2 μm in **F** and **I**.

Supplementary Fig. 7. IHC analyses of xenografts of human prostate cancer cells in embryonic zebrafish. **A-D:** Sections from zebrafish embryo with prostate cancer xenografts migrating to the tail region (**A-D**). Migrated cells are stained with H&E (**A-B**), and CK8-18 (**C-D**). **B-D** are higher magnification of the outlined area in **A**. **D** is a higher magnification of the outlined area in **C**. **E:** Localized xenograft outlined (**E**), and sections were stained with either H&E (**F**), or in dual IHC with the combination of PSA in red and hCD44 in brown (**G-H**). Notice the faint cytoplasmic red staining of PSA (arrows) with the overlying brown stating of hCD44. **F-H** are higher magnification of the outlined area in **E**. **H** is a higher magnification of the outlined area in **G**. Images were taken at 9 dpt for **A-D** and 8 dpf for **E-H**. Scale bars are 100 μm in **A** and **E**.

Supplementary Fig. 8. ELDA plot used to assess the frequency of self-renewing TICs. TIC frequencies were calculated using ELDA with 99% confidence interval. Correlation coefficient (R2) values are displayed. While the TIC potential for $\alpha2\beta1^{low}/CD44^{low}$ cells was limited (green lines), the 99% confidence interval for DU145 parental cells, and for $\alpha2\beta1^{hi}/CD44^{hi}$ cells sorted from 5-min-adherent fraction at correlation coefficient (R2) values of ≥0.99 were 1/175 to 1/338 and 1/75 to 1/125, respectively. This correlates to a frequency of self-renewing TIC of 0.296% to 0.57% in DU145 parental cells, and 0.8% to 1.33% in $\alpha2\beta1^{hi}/CD44^{hi}$ cells sorted from 5-min-adherent fraction. The overall frequency of

self-renewing TICs was calculated to be 0.3% to 1.3% of DU145 cells. These data were further confirmed using the L-calc software as described in supplemental methods. ELDA was used to assess the frequency of self-renewing tumor initiating PC3 and primary cells similarly (Not shown).

Supplementary Fig. 9. Xenotransplant of human prostate cancer cells in conditioned juvenile Casper zebrafish. **A**: Fluorescent image from a control untransplanted Casper zebrafish with background fluorescence within the gut region and in the eye. **B-E**: DU145 parental, 5-min adherent $\alpha2\beta1^{hi}$/$CD44^{hi}$ cells, and 20-min non-adherent $\alpha2\beta1^{low}$/$CD44^{low}$ cells were transplanted either SC in the tail region, or IP into 6-8 weeks Casper zebrafish. Recipient fish were conditioned with dexamethazone for 2 days before transplant. Non-tumor normal prostate cells were used as control and yielded no tumor formation (Supplementary Table 4). **B-C**: Representative fluorescent images from recipient fish transplanted with 5×10^2 parental DU145 cells SC (circled area) with tumor growth (**B**) and localized tumor spread (**C**) in the same fish at 13 and 28 dpt. The three right panels show both histology of the tumor growth in **B** (top), and 40X magnification of the circled area in **C** (middle panel is bright field and lower panel is 605 red fluorescence). **D-E**: A second representative fish from those transplanted with 5×10^1 5-min adherent $\alpha2\beta1^{hi}$/$CD44^{hi}$ sorted cells with tumor spread in the tail region (arrow in **E**) and to the brain (circled area above the eye in **E**). All images are lateral views with the zebrafish head to the left.

Supplementary Fig. 10. Metastatic behavior of prostate cancer cells *in vivo* in zebrafish xenografts. **A-H:** Histological sections stained with H&E from control untransplanted zebrafish muscle (**A-B**) and kidney marrow (**E-F**) tissues compared to matching sections from fish transplanted with the 5-min collagen-attached $\alpha2\beta1^{hi}$/$CD44^{hi}$ cells (**C-D** and **G-H**). Muscle section of control fish in low power (**A**) and high power (**B**) images demonstrates no cell infiltrates, while the corresponding muscle section of control fish in low power (**C**) and high power (**D**) images shows widespread tumor cell infiltrates (white arrow). Notice the round morphology of the DU145 engrafted cells compared to the elongated muscle nuclei. **E-H:** Histological H&E sections from a control non-transplanted juvenile zebrafish kidney marrow in **E**, and in higher power in **F** showing kidney tubules and marrow hematopoietic tissue (white arrow). The section from the DU145 TICs transplanted fish at day-13 post-transplant demonstrates fewer tubular structures, and tumor infiltrates and colonies of cells (black arrows) resembling the morphology of human DU145 tumor cells. **I:** Sections from muscle metastatic dissemination were subjected to IHC with anti-hCD44 demonstrating engrafted human DU145 cells. Data represent sections from recipient fish fixed at day 28 (n= 6/group). Scale bars are 50 μm in **A-H**, and 20 μm in **I**.

Table S1

DU145 Zebrafish Embryonic Transplant	Transplant embryos (Survivors)	Local growth	Dissemination potential (Presence of QD micro-metastasis at 3 dpt) (%)						
			Muscle	Yolk	Brain**	Micro-metastasis			
						<5	5-10	>10	Total [>5] tumor **(%)**
SC Vehicle	10 (9)	0 (0)	0 (0)	0 (0)	0 (0)	0 (0)	0 (0)	0 (0)	0 **(0)**
SC 10 cells									
Parental	50 (36)	4 (11)	19 (53)	18 (50)	12 (33)	2 (14)	10 (34)	15 (42)	25 **(69)**
Non-TICs	50 (38)	5 (13)	7 (18)	8 (21)	5 (13)	5 (14)	3 (61)	5 (14)	8 **(21)**
TICs	50 (40)	4 (10)	25 (62)	22 (55)	20 (40)	2 (40)	5 (40)	27 (40)	32 **(80)***
3 cells									
Parental	50 (42)	3 (7)	10 (24)	11 (26)	10 (24)	1 (42)	4 (42)	7 (42)	11 **(26)**
Non-TICs	50 (36)	0 (0)	6 (17)	5 (14)	2 (6)	2 (36)	2 (36)	4 (36)	6 **(17)**
TICs	50 (45)	3 (7)	20 (44)	20 (40)	17 (38)	2 (45)	2 (45)	20 (45)	22 **(49)***
SC 10 normal cells									
Parental	20 (17)	0 (0)	0 (0)	0 (0)	0 (0)	3 (18)	0 (0)	0 (0)	0 (0)
Non-TICs	20 (15)	0 (0)	0 (0)	0 (0)	0 (0)	2 (13)	0 (0)	0 (0)	0 (0)
Yolk 10 cells									
Parental	50 (44)	10 (23)	5 (11)	10 (23)	5 (11)	5 (44)	6 (44)	11 (44)	17 **(39)**
Non-TICs	50 (45)	15 (33)	1 (2)	2 (4)	0 (0)	3 (45)	2 (45)	2 (45)	4 **(9)**
TICs	50 (40)	13 (32)	8 (20)	14 (35)	6 (15)	3 (40)	8 (40)	14 (40)	22 **(55)***
3 cells									
Parental	50 (38)	5 (13)	3 (8)	7 (18)	3 (8)	4 (38)	4 (38)	7 (38)	11 **(29)**
Non-TICs	50 (42)	7 (17)	2 (5)	4 (10)	0 (0)	1 (42)	0 (42)	4 (42)	4 **(10)**
TICs	50 (42)	2 (5)	10 (24)	16 (38)	4 (10)	1 (42)	6 (42)	16 (42)	22 **(52)***

Table S1. Prostate tumor cell transplantation in embryonic zebrafish demonstrates tumor initiation potential of TICs. Embryos were transplanted in three independent experiments using 20 embryo/variable in two experiments, and 10 embryos/variable in a third experiment. Parental DU145 cells, non-collagen adherent cells at 20-min that were sorted for $\alpha2\beta1^{low}/CD44^{low}$ cells (Non-TICs), and 5-min collagen adherent cells that were sorted for $\alpha2\beta1^{hi}/CD44^{hi}$ (TICs) were injected either subcutaneously (SC) or into the yolk (Yolk) of 48-hpf zebrafish embryos at the indicated cell doses. Local tumor growth at the yolk resulted in an overall lower potential for tumor dissemination to distant sites compared to SC tumor growth, likely due to differences in nutritional microenvironments. Dissemination potential of injected cells in fish embryos was defined by the presence of migrating quantum dot (QD)-labeled cells at distant sites from the site of injection at 3-days post transplantation (dpt). Micro-metastasis was frequently detected at multiple distant sites simultaneously in the same embryo. The presence of >5 micro-metastasis sites was considered as an evidence for tumor growth and dissemination. Vehicle (PBS)- or QDs only-injected embryos did not develop any tumors. *TICs initiated significantly higher tumors than parental or non-TICs, ANOVA, $p< 0.001$ in all cell doses and injection sites. **Brain metastasis were present significantly higher in embryos injected with the TICs fraction, Fisher's exact test, $p< 0.001$. ***Tumor initiation potential of pretreated cells was significantly lower than untreated cells, n= ≥20, Fisher's exact test, $p< 0.02$.

Table S2

Prostate cancer Zebrafish Embryonic Transplant	Transplant embryos (Survivors)	Dissemination potential (Presence of QD micro-metastasis at 12 dpt) (%)
PC3 cells		
Adherent $\alpha2\beta1^{low}/CD44^{low}$	23 (18)	11 (61)*
Non-adherent $\alpha2\beta1^{hi}/CD44^{hi}$	22 (17)	6 (35)
Non-adherent $\alpha2\beta1^{low}/CD44^{low}$ (Non-TICs)	20 (18)	2 (11)
DU145 cells		
Adherent $\alpha2\beta1^{low}/CD44^{low}$	25 (19)	10 (53)
Non-adherent $\alpha2\beta1^{hi}/CD44^{hi}$	25 (23)	8 (35)
Non-adherent $\alpha2\beta1^{low}/CD44^{low}$ (Non-TICs)	25 (20)	7 (35)

Table S2. Tumor initiation potential of the different prostate cancer cell fractions from collagen-I adhesion. Embryos were transplanted in two independent experiments using >20 embryos/variable. Collagen-I-adherent cells and collagen-I-non-adherent PC3 and DU145 cells at 20-min were sorted for $\alpha2\beta1^{low}/CD44^{low}$ and $\alpha2\beta1^{hi}/CD44^{hi}$ cells. Sorted cells were injected into 48-hpf zebrafish embryos. The dissemination potential of injected cells into zebrafish embryos was defined by the presence of migrating labeled cells at distant sites from the injection site at 12 days post transplantation (dpt) to allow for testing the full range of tumor initiation. *PC3-adherent $\alpha2\beta1^{low}/CD44^{low}$ tumor initiation potential was significantly higher than non-TICs (Fisher's exact test, two-sided p-value=0.004). All other comparisons were not significantly different.

Table S3

Prostate cancer Zebrafish Embryonic Transplant		Transplant embryos (Survivors)	Dissemination potential (Presence of QD micro-metastasis at 3 dpt) (%)
PC3 cells			
	Parental	45 (37)	25 **(68)**
	Non-TICs	40 (30)	18 **(60)**
	TICs	32 (28)	24 **(86)**[1]
CWR22 cells			
	Parental	25 (18)	10 **(56)**
	Non-TICs	32 (24)	6 **(25)**
	TICs	45 (35)	22 **(63)**[2]
LnCap cells			
	Parental	30 (26)	17 **(65)**
	Non-TICs	20 (16)	10 **(62)**
	TICs	22 (20)	18 **(90)**[3]
Primary #2 cells			
	Parental	25 (18)	11 **(29)**
	Non-TICs	18 (15)	6 **(10)**
	TICs	20 (18)	15 **(52)**[4]
Primary #3 cells			
	Parental	23 (16)	14 **(87)**
	Non-TICs	22 (15)	13 **(87)**
	TICs	22 (19)	18 **(95)**[5]
Primary #6 cells			
	Parental	40 (36)	24 **(67)**
	Non-TICs	33 (25)	10 **(40)**
	TICs	45 (37)	32 **(87)**[6]

Table S3. Multiple prostate cancer cell lines and primary tumor cell transplantation in embryonic fish demonstrates tumor initiation potential of TICs. Embryos were transplanted in two independent experiments using >20 embryo/variable. Parental cells, non-collagen adherent cells at 20-min that were sorted for $\alpha2\beta1^{low}$/$CD44^{low}$ cells (Non-TICs), and 5-min collagen adherent cells that were sorted for $\alpha2\beta1^{hi}$/$CD44^{hi}$ (TICs) were injected SC in 48-hpf zebrafish embryos. The dissemination potential of injected cells in zebrafish embryos was defined by the presence of migrating quantum dot (QD)-labeled cells at distant sites from the site of injection at 3-days post transplantation (dpt). The presence of >5 micro-metastasis sites was considered an evidence for tumor growth and dissemination. Data from prostate cancer cell lines and three representative primary prostate cancer patient samples are demonstrated. [1]PC3-TICs were significantly higher than non-TICs, Fisher's exact test, two-sided p-value=0.04. [2]CWR22-TICs were significantly higher than non-TICs, Fisher's exact test, two-sided p-value=0.007. [3]LnCap-TICs showed a trend to be higher than non-TICs, Fisher's exact test, two-sided p-value=0.1034. [4]Primary-#2-TICs were significantly higher than non-TICs, Fisher's exact test, two-sided p-value=0.014. [5]Primary-#3-TICs were not significantly different from non-TICs, Fisher's exact test, two-sided p-value=0.57. [6]Primary-#6-TICs were significantly higher than non-TICs, Fisher's exact test, two-sided p-value=0.0002.

Table S4

	DU145 Juvenile Zebrafish Xenograft	Transplant zebrafish (Survivors)	Local growth	Dissemination potential (Presence of QD micro-metastasis at 28 dpt) (%)						
				Muscle	Marrow	Brain**	Micro-metastasis			
							<5	5-10	>10	Total [>5] tumor (%)
SC	**500 cells**									
	Parental	3 (3)	1 (33)	2 (67)	2 (67)	2 (67)	0 (0)	0 (0)	2 (67)	2 **(67)**
	Non-TICs	3 (3)	0 (0)	1 (33)	1 (33)	1 (33)	0 (0)	0 (0)	1 (33)	1 **(33)**
	TICs	3 (3)	1 (33)	3 (100)	2 (67)	2 (67)	0 (0)	0 (0)	3 (100)	3 **(100)**
	50 cells									
	Parental	3 (3)	0 (0)	3 (100)	3 (100)	3 (100)	0 (0)	0 (0)	3 (100)	3 **(100)**
	Non-TICs	3 (3)	0 (0)	0 (0)	0 (0)	0 (0)	0 (0)	0 (0)	0 (0)	0 **(0)**
	TICs	3 (3)	1 (33)	3 (100)	3 (100)	3 (100)	0 (0)	0 (0)	2 (67)	3 **(100)**
	10 cells									
	Parental	3 (2)	0 (0)	2 (67)	1 (33)	0 (0)	0 (0)	0 (0)	2 (67)	2 **(67)**
	Non-TICs	3 (3)	0 (0)	1 (33)	1 (33)	1 (33)	0 (0)	0 (0)	1 (33)	1 **(33)**
	TICs	3 (3)	0 (0)	2 (67)	2 (67)	2 (67)	0 (0)	0 (0)	2 (67)	2 **(67)**
IP	**500 cells**									
	Parental	3 (3)	2 (67)	1 (33)	0 (0)	0 (0)	0 (0)	0 (0)	1 (33)	3 **(100)**
	Non-TICs	3 (3)	0 (0)	1 (33)	0 (0)	0 (0)	0 (0)	0 (0)	1 (33)	1 **(33)**
	TICs	3 (3)	1 (33)	3 (100)	2 (67)	2 (67)	0 (0)	1 (33)	1 (33)	2 **(67)**
	50 cells									
	Parental	3 (3)	1 (33)	2 (67)	1 (33)	3 (100)	0 (0)	1 (33)	1 (33)	3 **(100)**
	Non-TICs	3 (3)	0 (0)	0 (0)	0 (0)	0 (0)	0 (0)	0 (0)	0 (0)	0 **(0)**
	TICs	3 (3)	0 (0)	3 (100)	3 (100)	3 (100)	0 (0)	1 (33)	2 (67)	3 **(100)**
	10 cells									
	Parental	3 (3)	0 (0)	2 (67)	1 (33)	0 (0)	0 (0)	1 (33)	0 (0)	1 **(33)**
	Non-TICs	3 (3)	0 (0)	0 (0)	0 (0)	0 (0)	0 (0)	0 (0)	0 (0)	0 **(0)**
	TICs	3 (3)	1 (33)	2 (67)	2 (67)	2 (67)	0 (0)	0 (0)	2 (67)	3 **(100)***

Table S4. Prostate tumor cell transplantation in juvenile conditioned zebrafish demonstrates the metastatic potential of TICs. Juvenile 6-8 week zebrafish were conditioned with 10 μg/ml dexamethazone for 2 days as described [28]. On the next morning, fish were anesthetized with tricaine, and transplanted in three independent experiments using 9 juvenile fish/cell dose. QD-labeled parental DU145 cells, non-collagen adherent cells at 20-min that were sorted for $\alpha2\beta1^{lo}/CD44^{lo}$ cells (Non-TICs), and 5–min collagen adherent cells that were sorted for $\alpha2\beta1^{hi}/CD44^{hi}$ cells (TICs) were injected either SC in the tail region, or IP at the indicated cell doses. The dissemination potential of injected cells in zebrafish was defined by the presence of migrating QD-labeled cells at distant sites from

the site of injection at days 13- and 28-dpt. The presence of >5 micro-metastasis sites was considered as an evidence for tumor growth and metastasis. Dissemination was frequently detected at multiple distant sites including brain, muscle, and kidney marrow with multiple colonies detected simultaneously after local growth in the same recipient zebrafish. Vehicle (PBS)- or QDs only-injected fish did not develop any tumors. *TICs initiated significantly higher tumors than parental or non-TICs, ANOVA, $p < 0.001$ in all doses and injection sites. **Brain metastases were present at a significantly higher rate in fish injected with the TICs fraction, Fisher's exact test; $p < 0.001$.

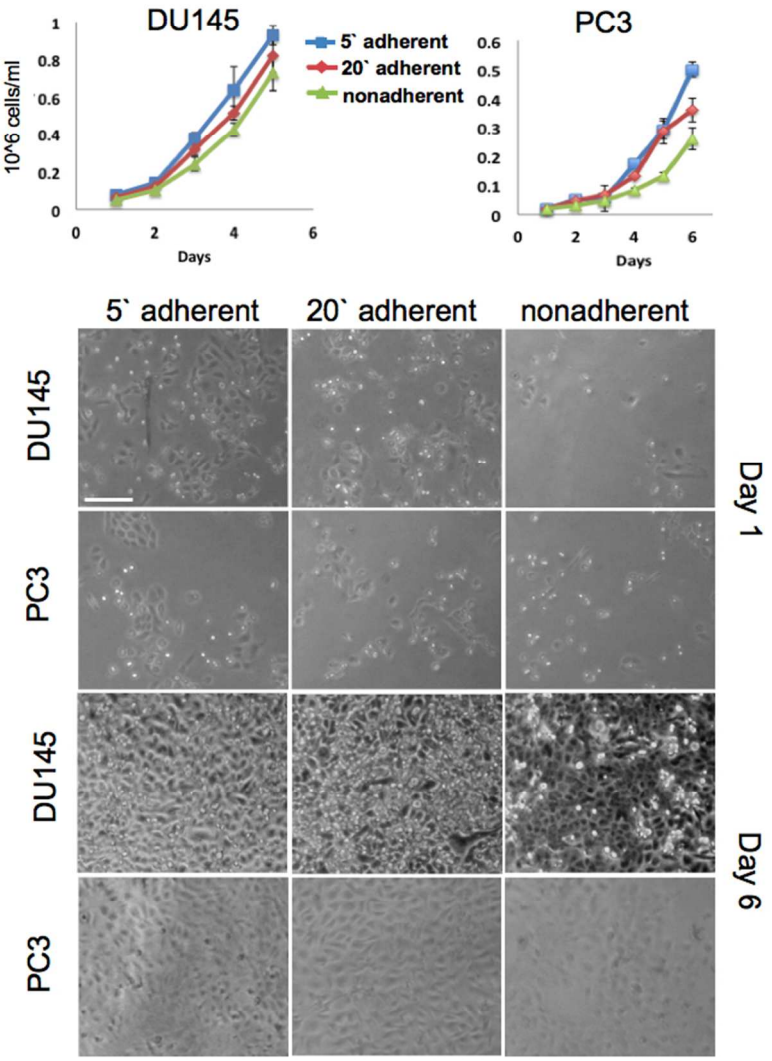
DU145
PC3
5` adherent
20` adherent
nonadherent
10^6 cells/ml
Days
5` adherent
20` adherent
nonadherent
DU145
PC3
DU145
PC3
Day 1
Day 6

FigS1

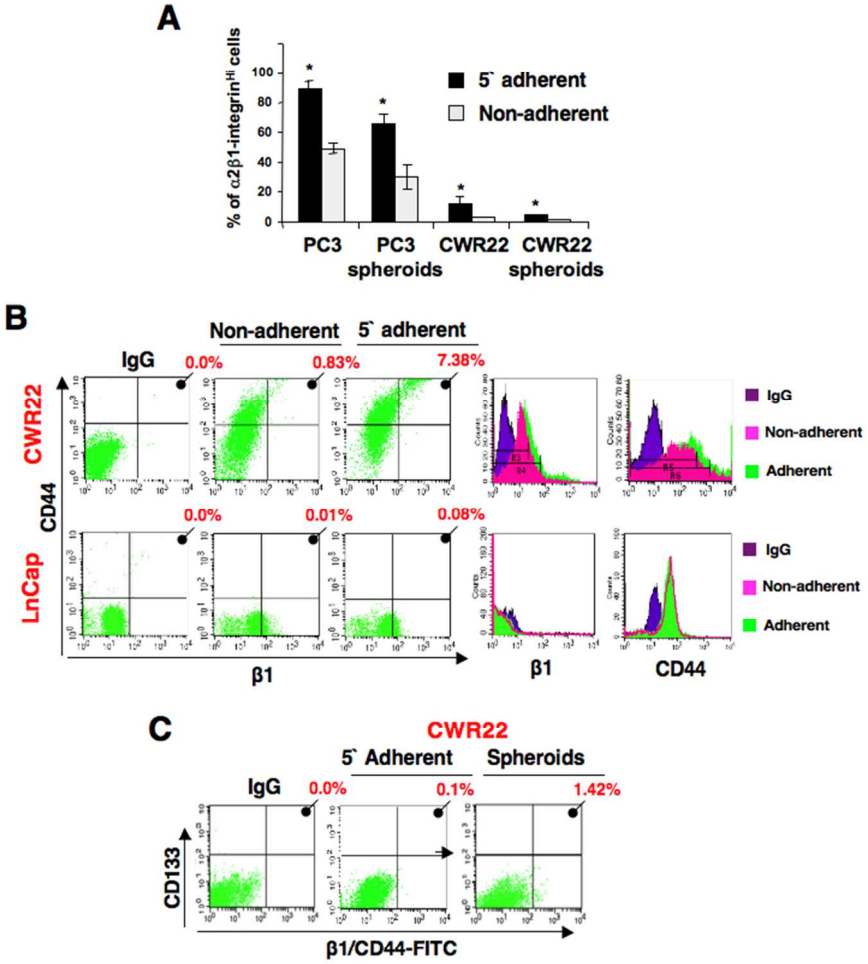
A
% of α2β1-integrin^Hi cells
100
80
60
40
20
0
5` adherent
Non-adherent
PC3
PC3 spheroids
CWR22
CWR22 spheroids
B
Non-adherent
5` adherent
IgG
0.0%
0.83%
7.38%
CWR22
CD44
LnCap
0.0%
0.01%
0.08%
β1
IgG
Non-adherent
Adherent
β1
CD44
C
CWR22
5` Adherent
Spheroids
IgG
0.0%
0.1%
1.42%
CD133
β1/CD44-FITC

FigS2

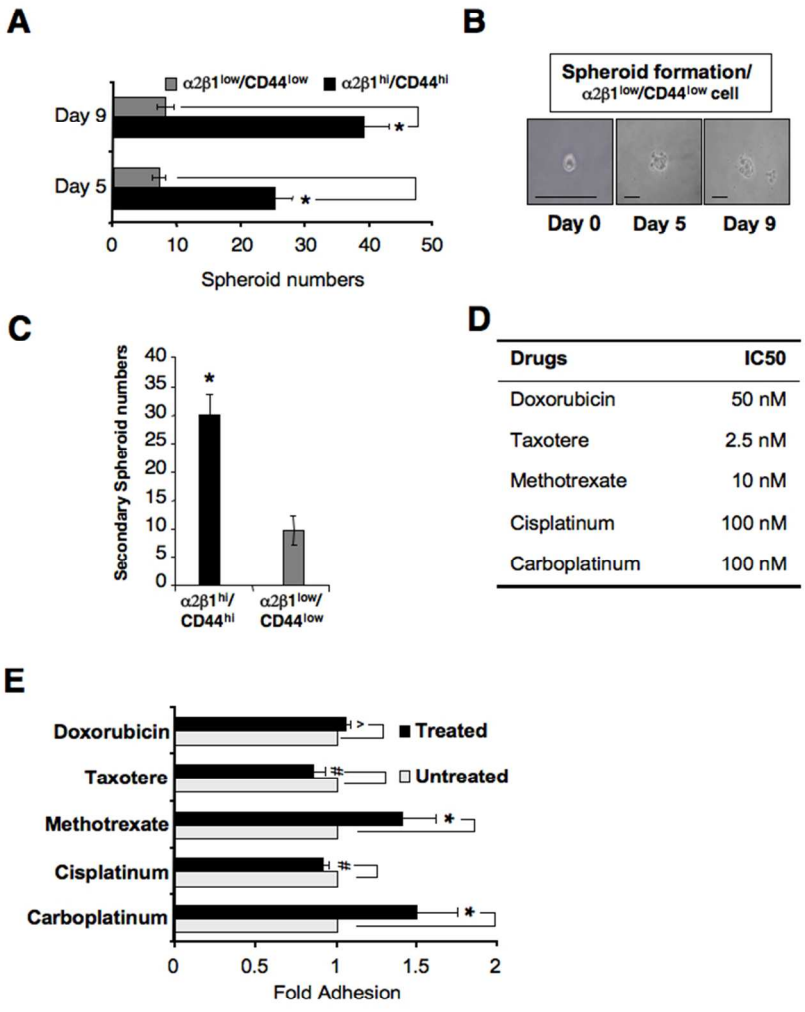
A
α2β1low/CD44low
α2β1hi/CD44hi
Day 9
Day 5
0 10 20 30 40 50
Spheroid numbers
B
Spheroid formation/
α2β1low/CD44low cell
Day 0
Day 5
Day 9
C
Secondary Spheroid numbers
0 5 10 15 20 25 30 35 40
α2β1hi/ CD44hi
α2β1low/ CD44low
D
Drugs IC50
Doxorubicin 50 nM
Taxotere 2.5 nM
Methotrexate 10 nM
Cisplatinum 100 nM
Carboplatinum 100 nM
E
Doxorubicin
Taxotere
Methotrexate
Cisplatinum
Carboplatinum
Treated
Untreated
0 0.5 1 1.5 2
Fold Adhesion

FigS3

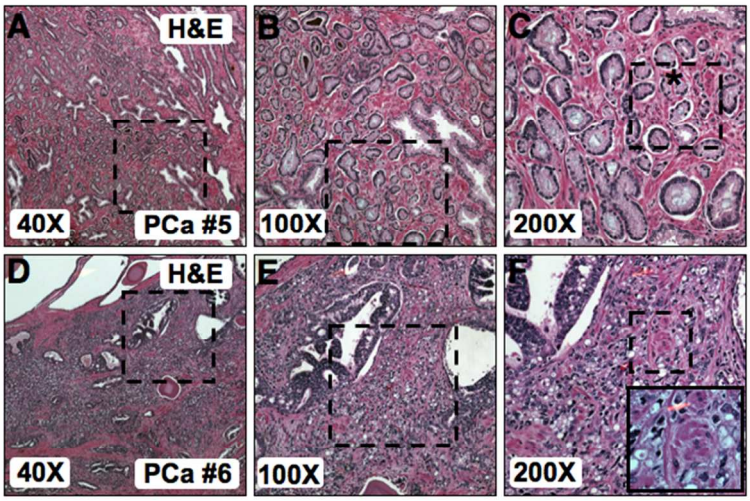

FigS4

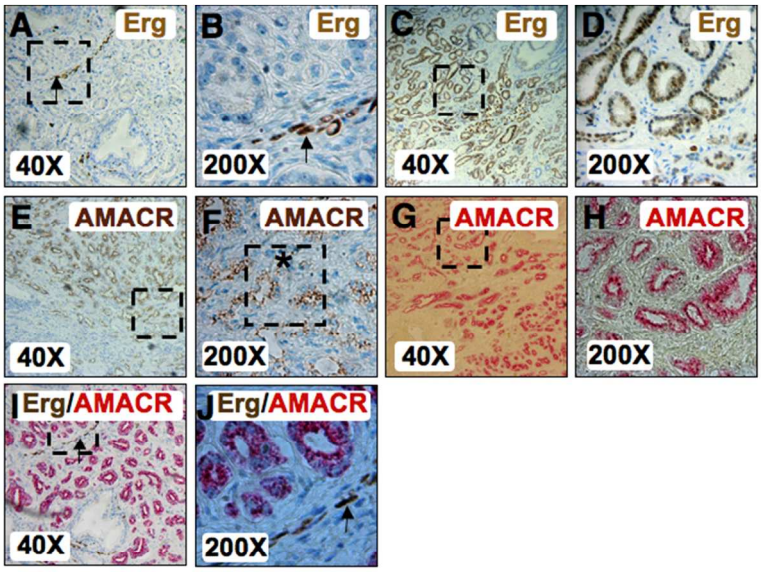
A
Erg
40X
B
Erg
200X
C
Erg
40X
D
Erg
200X
E
AMACR
40X
F
AMACR
200X
G
AMACR
40X
H
AMACR
200X
I
Erg/AMACR
40X
J
Erg/AMACR
200X

FigS5

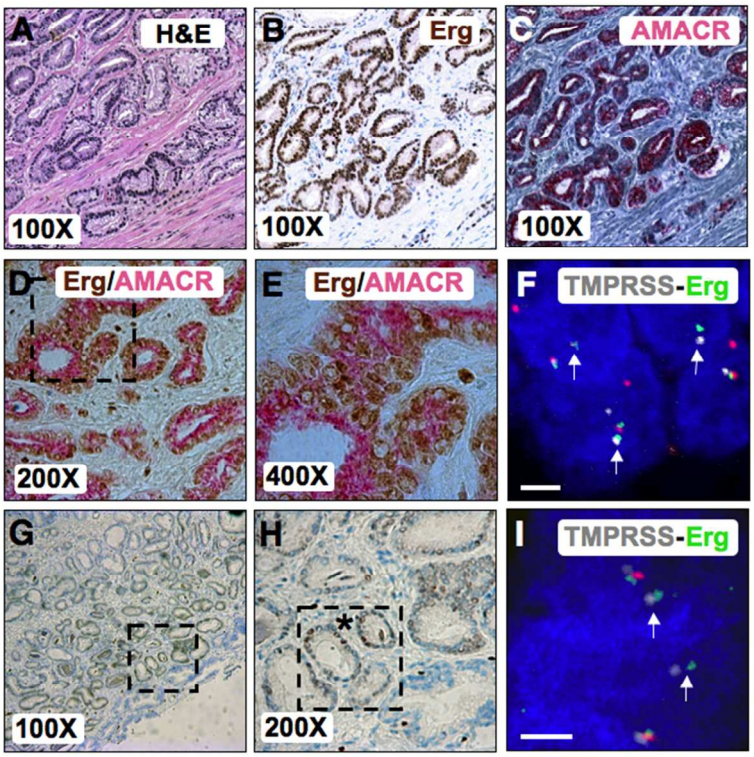
A
H&E
100X
B
Erg
100X
C
AMACR
100X
D
Erg/AMACR
200X
E
Erg/AMACR
400X
F
TMPRSS-Erg
G
100X
H
*
200X
I
TMPRSS-Erg

FigS6

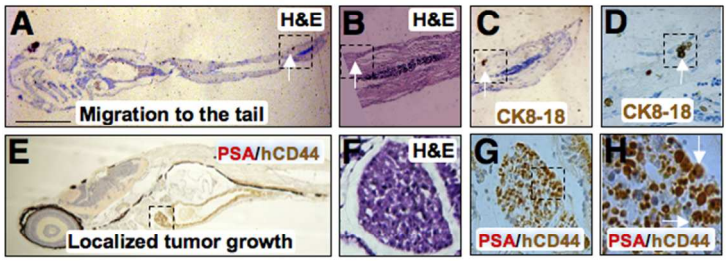
A
H&E
Migration to the tail
B
H&E
C
CK8-18
D
CK8-18
E
PSA/hCD44
Localized tumor growth
F
H&E
G
PSA/hCD44
H
PSA/hCD44

FigS7

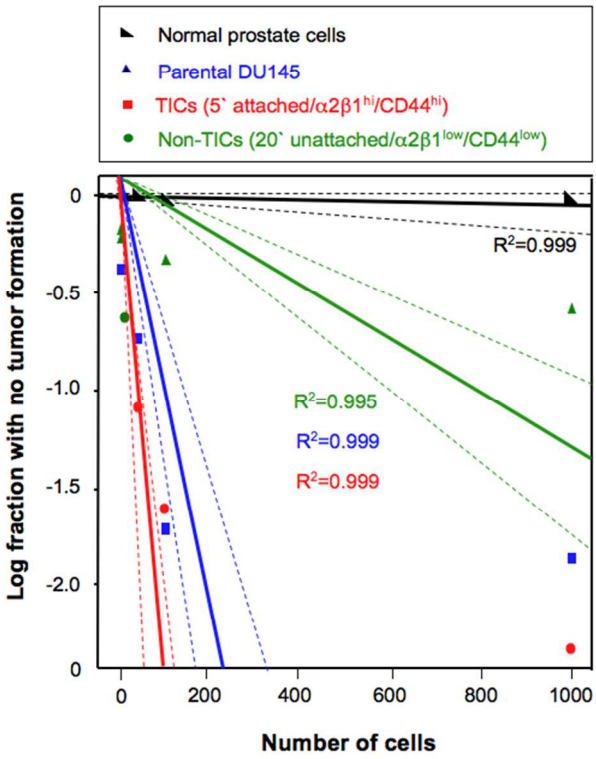
Normal prostate cells
Parental DU145
TICs (5` attached/α2β1hi/CD44hi)
Non-TICs (20` unattached/α2β1low/CD44low)
Log fraction with no tumor formation
0
-0.5
-1.0
-1.5
-2.0
0
R2=0.999
R2=0.995
R2=0.999
R2=0.999
0
200
400
600
800
1000
Number of cells

FigS8

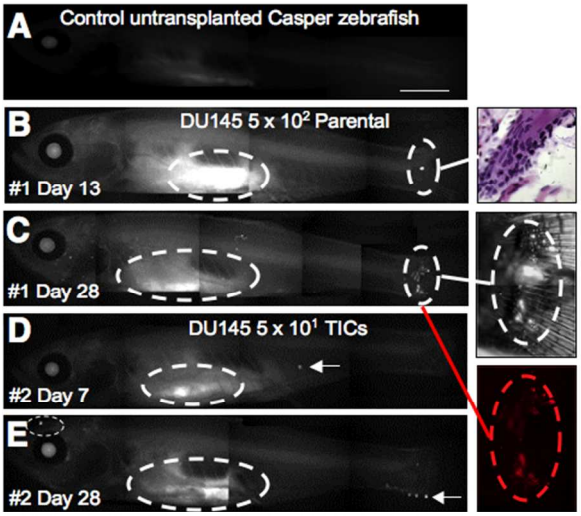
A
Control untransplanted Casper zebrafish
B
DU145 5 x 10² Parental
#1 Day 13
C
#1 Day 28
D
DU145 5 x 10¹ TICs
#2 Day 7
E
#2 Day 28

FigS9

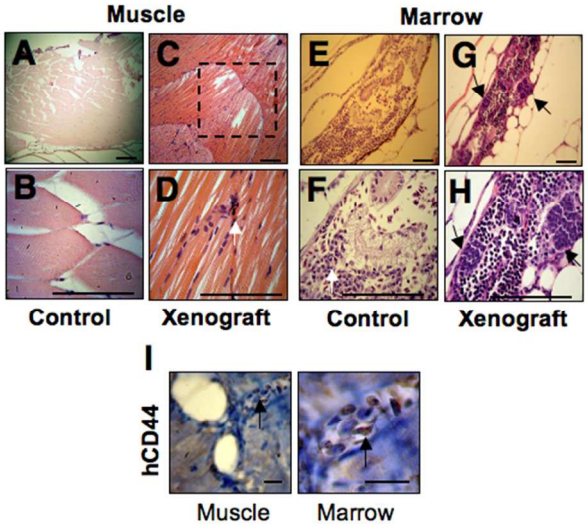
Muscle
Marrow
A
C
E
G
B
D
F
H
Control
Xenograft
Control
Xenograft
I
hCD44
Muscle
Marrow

FigS10